Denudation of the Golan Heights basaltic terrain using in-situ 36Cl and OSL dating

Yaron Be'Eri-Shlevin, Ari Matmon, Rotem Rotstein, I. Schimmelpfennig, Lucilla Benedetti, Yona Geller, Porat Naomi, Noam Greenbaum, Team Aster

Journal Pre-proof

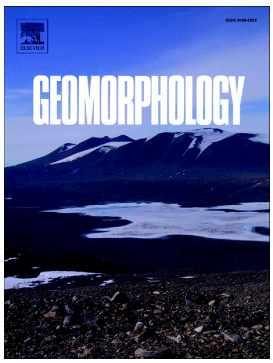

Denudation of the Golan Heights basaltic terrain using in-situ 36Cl and OSL dating

Yaron Be'eri-Shlevin, Ari Matmon, Rotem Rotstein, Irene Schimmelpfennig, Lucilla Benedetti, Yona Geller, Porat Naomi, Noam Greenbaum, ASTER Team

PII: S0169-555X(23)00069-7

DOI: https://doi.org/10.1016/j.geomorph.2023.108649

Reference: GEOMOR 108649

To appear in: *Geomorphology*

Received date: 22 September 2022

Revised date: 6 March 2023

Accepted date: 6 March 2023

Please cite this article as: Y. Be'eri-Shlevin, A. Matmon, R. Rotstein, et al., Denudation of the Golan Heights basaltic terrain using in-situ 36Cl and OSL dating, *Geomorphology* (2023), https://doi.org/10.1016/j.geomorph.2023.108649

Denudation of the Golan Heights basaltic terrain using in-situ ^{36}Cl and OSL dating

Be'eri-Shlevin Yaron[1], Matmon Ari[2], Rotstein Rotem[1,3], Schimmelpfennig Irene[4], Benedetti Lucilla[4], Geller Yona[2], Naomi Porat[5], Greenbaum Noam[3], ASTER Team[6]

1) The Kinneret Limnological Laboratory, Israel Oceanographic and Limnological Research, Migdal 14950, Israel.

2) The Fredy and Nadine Herrmann Institute of Earth Sciences, Edmond J. Safra Campus, Givat Ram, Jerusalem 91904, Israel.

3) The Department of Geography and Environmental studies, University of Haifa, Haifa 31905, Israel.

4) Aix-Marseille Université, Centre National de la Recherche Scientifique (CNRS)–Institut de Recherche pour le Développement IRD)–Collège de France, UM 34 Centre de Recherche et d'Enseignement de Géosciences de l'Environnement (CEREGE), Technopôle de l'Arbois, BP80, 13545 Aix-en-Provence, France.

5- The Geological Survey of Israel, 32 Yesha'ayahu Leibowitz St., Jerusalem, 9692100, Israel

6-Centre de Recherche et d'Enseignement de Géosciences de l'Environnement (CEREGE), Technopôle de l'Arbois, BP80, 13545, Aix-en-Provence, France

Abstract

While erosion rates of carbonates along the Dead Sea fault (DSF) and its margins have been determined in several studies, information about denudation of basalts along the DSF are absent. Here we report concentrations of in situ cosmogenic ^{36}Cl in bedrock and sediment samples combined with OSL ages of terraces from the Meshushim basin, a typical basaltic basin in the Golan Heights, northern Dead Sea Rift (DSR).

Denudation rates of exposed and soil-covered bedrock basalts range from 12.3±1.4 mm/ka to 176.1±47.4 mm/ka, well within the range of DSR values, regardless of lithology and climate. In all locations where exposed and soil-covered bedrock were samples next to each other, the soil-covered basalt erodes faster. This is regardless of notable variations in average annual temperature and precipitation. This means that bedrock outcrops were not covered and exposed very frequently, and that chemical weathering at the bedrock-soil interface is a significant erosional factor.

Sediments in the Meshushim basin are stored in soil pockets and blankets on the upper plateau, colluvial material on slopes, and alluvial terraces. The difference in ^{36}Cl concentrations between soil-covered and exposed bedrock indicates coverage duration of ca. 3-6 ka. The residence time estimate of only several thousands of years for sediments stored in alluvial terraces is 170±20 y to 4000±290 y. Nowhere in the Meshushim drainage system did we find evidence for storage of sediment longer than a few thousands of years.

^{36}Cl concentrations in colluvial and alluvial sediments are similar to those measured in soil-covered basalts. This similarity suggests that sub-surface weathering of basalts is the major source for sediments in upper and central segments of the basin, concurrent with the higher denudation rates of buried bedrock. However, very low ^{36}Cl concentrations measured in samples collected in the lower parts of the basin indicate involvement of landslides which instantaneously expose previously shielded sediments that were incorporated into the drainage system. The effect of landslides is also

manifested by the high basin scale denudation rates calculated from alluvial samples in various locations, as well as the geomorphological profile of the Meshushim basin. Sediment yield calculated from ^{36}Cl concentrations measured in this study suggest temporal changes in denudation rates over the Holocene and up to the last ~60 ka, with higher past denudation rates and sediment yield even in most of the Holocene related to present rates and yields.

Overall, the results of this study show that the fact that the Golan lithology is basaltic does not result in different denudation process and rate from other locations investigated along the Dead Sea Rift, which are mostly of carbonate lithology and that relief and climate are stronger parameters than lithology in controlling denudation.

1. Introduction

Landscapes reflect the balance between the competing processes of tectonic uplift and subsidence and surface processes, which are manifested, in a general way, by denudation (e.g., Bull, 1991; Pazzaglia, 2013). Denudation, the lowering of the earth's surface, is one of the most important processes that control landscape evolution (Barreto et al., 2013). The term "denudation" refers to all physical erosion and chemical weathering processes combined. Bedrock weathering and erosion, incision of alluvial channels and removal of material down slopes into channels are among the processes that contribute to denudation.

Numerous studies in a wide range of environments have promoted our understanding of the roles of base-level, lithology, structure, and climate in controlling the evolution of landscapes and in determining the rate at which bedrock surfaces erode (e.g., Molnar and England, 1990; Burbank et al., 1996; Riebe et al., 2001; Sklar and Dietrich, 2001; Hancock and Anderson, 2002; Anders et al., 2006; Di Biase and Whipple, 2011; Benedetti et al., 2016). Bedrock erosion rates around the world range over 4 orders of magnitude, between >1000 mm/ka in orogenic mountain belts under very

humid climatic conditions to <1mm/ka in the most arid and flat surfaces of the world. Still, of the eroding parts of the Earth's surface, most erode at rates of 25-75 mm/ka (Matmon et al., 2009; 2017; Portenga and Bierman, 2011, Bierman et al., 2014).

Denudation rates are affected by rock type, tectonic setting, and climatic conditions, mainly temperature and amount of precipitation (e.g., Schumm and Lichty, 1965; Leopold and Bull, 1979; Schumm, 1973, 1981; Molnar and England, 1990; Bull, 1991; Pazzaglia, 2013; Gran et al., 2013). Various studies show that denudation in silicate terrains is mostly affected by tectonic uplift and the resulting relief (e.g., Perron, 2017), while in carbonate terrains denudation is more sensitive to climatic variations (e.g., Ryb et al., 2014a, 2014b; Avni et al., 2018).

In this study, we determine denudation rates and sediment transport and yield in a basaltic terrain, the Golan Heights, along an active plate boundary, the Dead Sea fault, under semi humid to semiarid climatic gradient. Between the Gulf of Aqaba in the south and Mt. Hermon in the north of Israel (a distance of ~500 km, **Fig. 1**), the Golan Heights are the only basaltic terrain that drains into the DSR. The Golan Heights thus provide an excellent opportunity to investigate the impact of an active subsiding base level on erosion of basaltic bedrock and the incision of channels into a basaltic plateau. Furthermore, a comparison of bedrock erosion, sediment yield and incision rates in this basaltic terrain with carbonate terrains, also situated along the Dead Sea rift under the same climatic conditions, provides insight regarding the effect of lithology on the rates of surface processes. This is a unique tectonic-climatic-lithologic setting that has not been investigated. We apply in-situ cosmogenic ^{36}Cl analyses and optically stimulated luminescence (OSL) dating in samples collected from various geomorphic positions in the Meshushim drainage system, that drains the basaltic terrain of the Golan Heights into the Sea of Galilee, Israel (**Fig. 1**). We analyze samples from several morphologic settings: alluvial and colluvial sediments and exposed and buried bedrock samples. OSL and in-situ cosmogenic isotope exposure dating methods help understand different surface processes. The combination of these two dating methods has proved in the past to yield valuable

insights into surface processes and landscape evolution (e.g., Guralnik et al., 2011; Fruchter et al., 2011; Rinat et al., 2014; Matmon et al., 2016; Neagu et al., 2020).

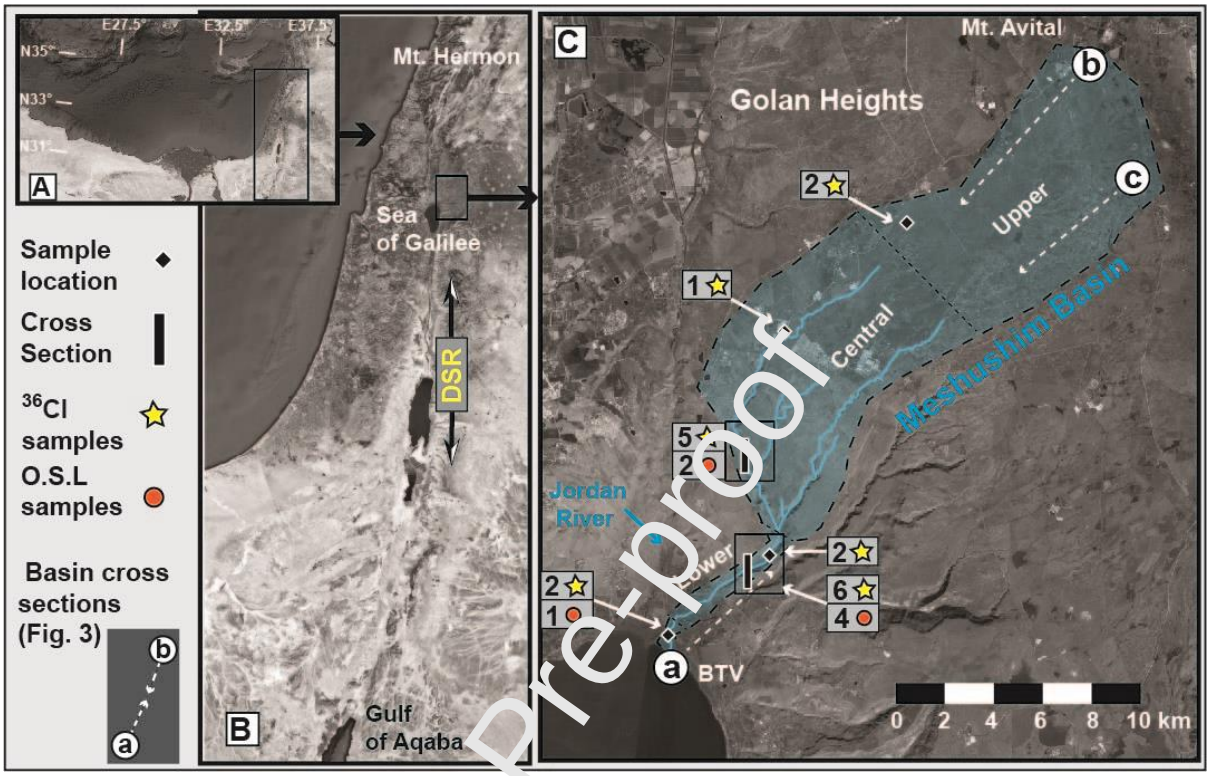

Fig. 1: Location map of study area. (A) the Eastern Mediterranean; (B) the Dead Sea Rift; (C) The Golan Heights and Meshushim basin with its division into different segments. A DEM map of the same area in displayed in **Fig. 2**. The location of basin cross sections which are presented in **Fig. 3** (a-b and a-c) are marked by dashed white arrows. Sampling locations are marked by black solid diamonds, and elongated rectangles, the latter designating a set of samples along a study cross section, with black squares indicating locations of images in **Fig. 4**. Type (OSL- red circles, ^{36}Cl- yellow stars), and the number of samples per sampling site are designated. BTV-MS: Location of long-term monitoring stations.

1.1. Study area

The Golan Heights are a young basaltic plateau that slopes from an altitude of 1200-1400 m asl in the north to about 200 m asl in the southeast where it is bordered by an escarpment overlooking

the Sea of Galilee and the Dead Sea Rift (DSR), which are located at ~210 meters below sea level (**Figs. 1, 2**). The basalt rocks exposed on the plateau range in age from the early Pliocene to late Pleistocene (Mor, 1993; Heimann et al., 1996; Weinstein et al., 2006, 2020; Behar et al., 2019). The basalts in the northern Golan are younger than the ones in the south and the thickness of the basalt cover also increases from tens of meters in the south to hundreds of meters in the north (Mor, 1993).

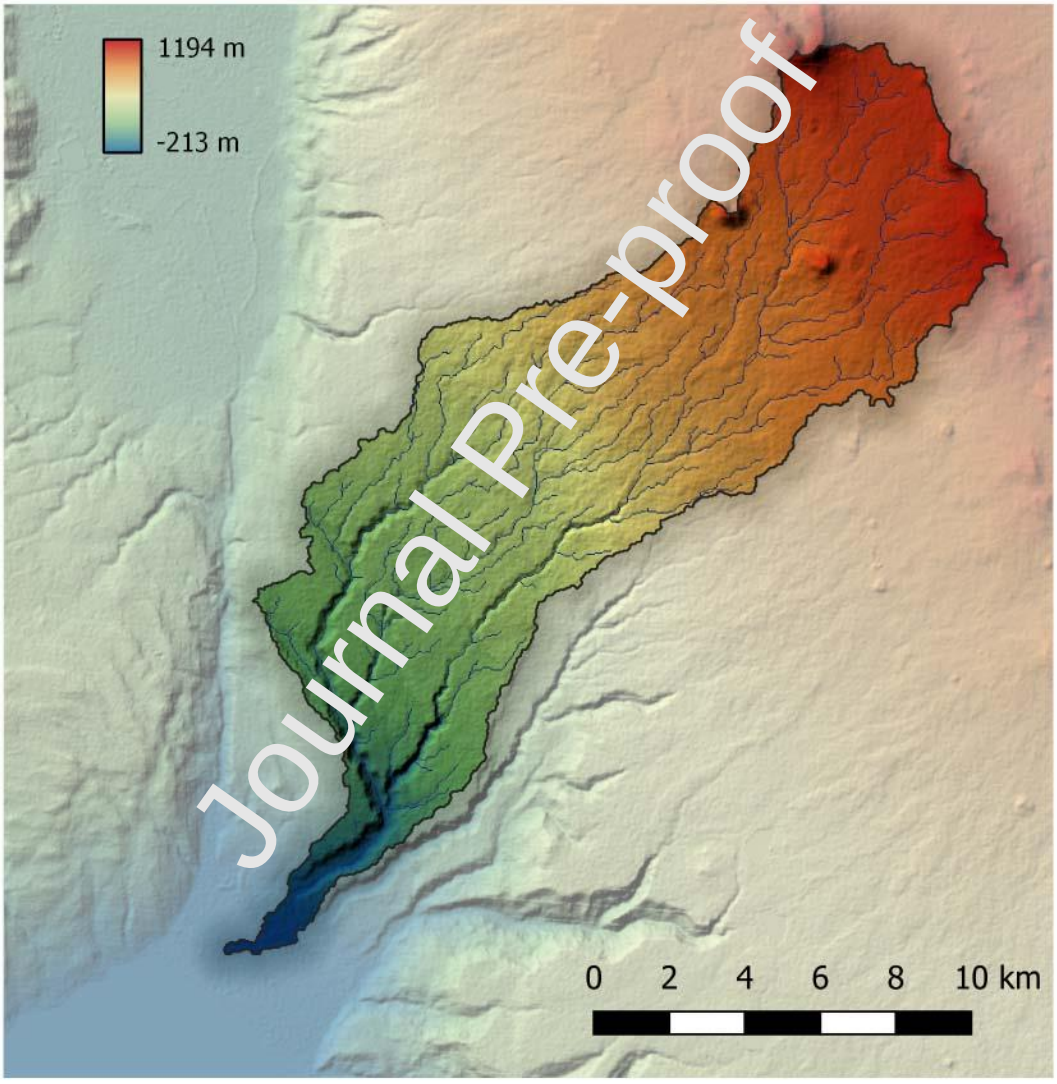

Figure 2: A digital elevation map (DEM) for the Meshushim Basin.

The Meshushim Stream basin is the second largest stream flowing into the Sea of Galilee from the Golan Heights, second only to the Jordan River. The Meshushim basin drains an area of

approximately 160 km². Its main stream channel is ~45 km long, most of its creeks are ephemeral but some parts are fed by springs and therefore are perennial. The head of the basin is located at the east of the Golan Heights plateau near Mt. Avital (1208 m asl; **Figs. 1, 2**) and the main channel flows south-west to Beit Tzaida Valley (BTV) at 210 m bsl. The average slope of the stream is 3% (**Fig. 3**; Grodek, 1994). Two main knickpoints are located within the Meshushim basin: one in the main stream of the Meshushim and the second in the Zavitan Stream (the main tributary of the Meshushim Stream). The Zavitan Stream is characterized by a steeper gradient than the Meshushim Stream and the section below the knickpoint includes a narrow canyon several tens of meters deep (**Fig. 3**). In contrast, the Meshushim Stream is characterized below the knickpoint by a 1 km wide river valley. Based on the morphology of the thalweg and slopes, the Meshushim basin is divided here into 4 main segments in accordance with Inbar (2012): Upper, Central, Lower, and BTV (Beit Tzeida Valley; **Fig. 1**) - a tectonic valley which hosts the common delta of the Jordan River, the Meshushim, and other streams (Ben-Avraham et al., 1996; Meiler et al., 2011). Several studies were conducted regarding modern sediment transport in the Meshushim stream (Inbar and Schick, 1979; Grodek, 1994; Inbar, 2000; 2012; Bergman et al., 2018; 2021). Overall, these studies show that modern peak flows had the capacity to transport boulder sizes up to 1.3m.

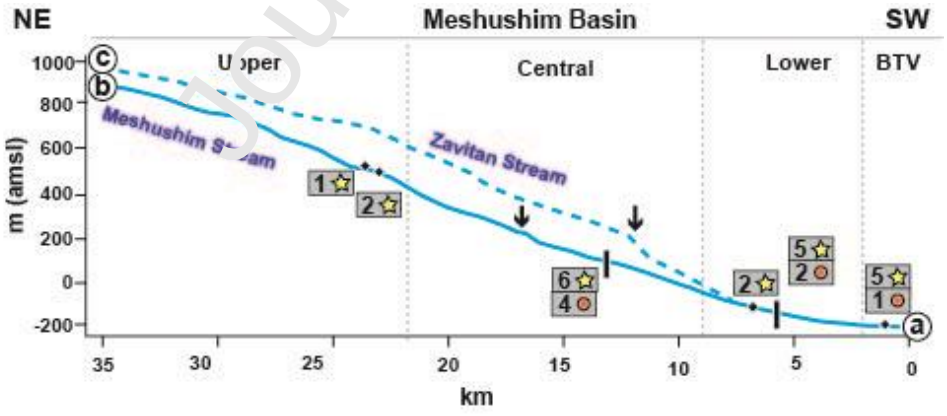

Fig. 3: Basin cross sections (modified from Inbar, 2012) of the Meshushim and Zavitan streams within the Meshushim basin with location and number of OSL and ^{36}Cl samples as in **Fig. 1**. Vertical black arrows denote Knickpoint locations in both streams.

2. Methods

2.1 In situ cosmogenic chlorine-36 (^{36}Cl)

Over the last three decades, cosmogenic nuclides have been widely used to determine denudation rates in various terrains (Dunai, 2010; Bierman, 1994). ^{36}Cl (half-life = 3.1 x 10^5 y; Bierman et al., 1995) is one of the most studied and useful cosmogenic nuclides for quantifying surface processes (Bierman et al., 1995; Schimmelpfennig et al., 2009; Schimmelpfennig et al., 2011). It is formed both in the atmosphere and in the lithosphere through various production path ways (Gosse and Phillips, 2001) and in a wide range of minerals and rocks (Bierman et al., 1995). This creates some complexity in the interpretation of ^{36}Cl concentrations. In order to interpret measured ^{36}Cl concentrations, it is necessary to identify and measure all its production pathways (Schimmelpfennig et al., 2011). Another problem is the lack of consensus regarding ^{36}Cl production rates (PR), although, in recent years, much progress has been made in ^{36}Cl methodology and it has been proven that it is now possible to overcome many obstacles that existed in the past (Zreda et al., 1991; Licciardi et al., 2008, Schimmelpfennig et al., 2009; Schimmelpfennig et al., 2011).

Generally, analysis of ^{36}Cl is applied to Ca-rich rocks such as carbonate rocks (Gran et al., 2001; Benedetti et al., 2002; Palumbo et al., 2004; Haviv et al., 2006; Schlagenhauf et al., 2010; Benedetti et al., 2013; Ryb at al., 2014a, b; Thomas et al., 2017; Avni et al., 2018; Mozafari et al., 2019). Although it is also commonly used for investigating the exposure and erosion history of basaltic rocks (e.g., Alcalá-Reygosa et al., 2018; Groos et al., 2021; Phillips et al., 1990; Jomelli et al.,

2016; Fernández-Fernández et al., 2019; Charton et al., 2022) it has not been extensively applied in denudation studies of basaltic terrains.

In this study we used ^{36}Cl concentrations in basaltic samples collected from the Meshushim basin to determine site specific and basin wide denudation rates, as well as basin sediment yield. All together we collected in this study 18 samples of basalt composition for ^{36}Cl analysis (**Figs. 1,3,4; Table 1**): (1) exposed and soil-covered bedrock samples (n=6), collected along the uppermost parts of the slopes above each segment of the Meshushim basin, (2) colluvium samples (n=4), (3) coarse alluvial samples (n=4) and, (4) fine alluvial samples (n=4) composed of <1 mm basaltic fragments that were sieved from fine grained alluvial sediment. The colluvial and coarse alluvial samples were composed of ~30 amalgamated small clasts, 1-3 cm in diameter, that were collected from the surface. Colluvial and alluvial samples were mostly collected along two valley cross-sections including slopes and alluvial terraces, as well as in the Meshushim delta site within the BTV (**Figs. 1,3,4, Supplementary Figure 1**).

Chlorine was extracted from the basalt sample grains at the "Laboratoire National des Nucléides Cosmogéniques" (LN2C) at CEREGE, Aix-en-Provence, France, following the methods described in Schimmelpfennig (2009). Isotopic measurements were conducted at the ASTER AMS, CEREGE, Aix en Provence, France (Arnold et al., 2013). ^{36}Cl/^{35}Cl ratios were normalized to the inhouse standard SM-CL-12 using an assigned value of 1.428 (±0.021) x 10^{12} (Merchel et al., 2011), while a natural ratio of 3.127 was assumed for the stable ^{35}Cl/^{37}Cl ratio. From these ratios, the ^{36}Cl and Cl concentrations were calculated following the equations in Schimmelpfennig (2009) (**Table 2**). Blank correction was performed by subtracting the number of Cl and ^{36}Cl atoms in the blank from those of the samples.

According to standard methods (Schimmelpfennig, 2009), aliquots of the basalt sample grains were put aside for compositional analyses, required for the determination of site-specific production

rate and ^{36}Cl concentrations. Due to technical problems related to the analyses of the major and some trace elements, average concentrations calculated by Weinstein et al. (2006) were used (**Supplement Table 1**). Considering the homogeneous major element concentration, characterizing the late Pliocene to late Pleistocene basalts from this area as reported by Weinstein et al. (2006), using these average concentrations seems feasible for the purposes of the current work. Concentrations of the following trace elements (U, Th, Ba, Li, Gd) were obtained by ICP-MS measurements conducted at the Institute of Earth Sciences, Hebrew University of Jerusalem, Israel (**Supplement Table 2**). To calculate the steady state erosion rates, we used the calculation spreadsheet by Schimmelpfennig et al. (2009).

In all calculations, we use the time-invariant scaling method by Stone (2000) and sea level high latitude production rates of 42.2 ± 4.8 atoms of ^{36}Cl (g Ca)$^{-1}$ yr^{-1} for Ca spallation (Schimmelpfennig et al., 2011), 148.1 ± 7.8 atoms of ^{36}Cl (g K)$^{-1}$ yr^{-1} for K spallation (Schimmelpfennig et al., 2014), 13 ± 3 atoms of ^{36}Cl (g Ti)$^{-1}$ yr^{-1} for spallation of Ti (Fink et al., 2000), 1.9 ± 0.2 atoms of ^{36}Cl (g Fe)$^{-1}$ yr^{-1} for Fe spallation (Stone et al., 2005), and 690 ± 185 neutrons (g air)$^{-1}$ yr^{-1} for the rate of epithermal neutron production from fast neutrons (Marrero et al., 2016). Although time-invariant, we use the scaling method of Stone (2000) because it is embedded in the Schimmelpfennig et al. (2011) erosion rate/exposure age calculation procedure. It should be noted that scaling models that account for paleo-geomagnetic intensity changes yield very similar mean values (at most +4%), therefore, not altering our results and interpretations. We applied a value of 160 g cm^2 for the high-energy neutron attenuation length. Overburden density was 2.7 g/cm^3 for exposed samples and 1.8 g/cm^3 for soil covered ones (**Table 1**).

^{36}Cl concentrations measured in alluvial samples were interpreted in terms of weighted average basin wide erosion upstream of the sampling location. Weighted average scaling factors for basin wide erosion rates were calculated considering the hypsometric curve of the basin area above each alluvial sample location.

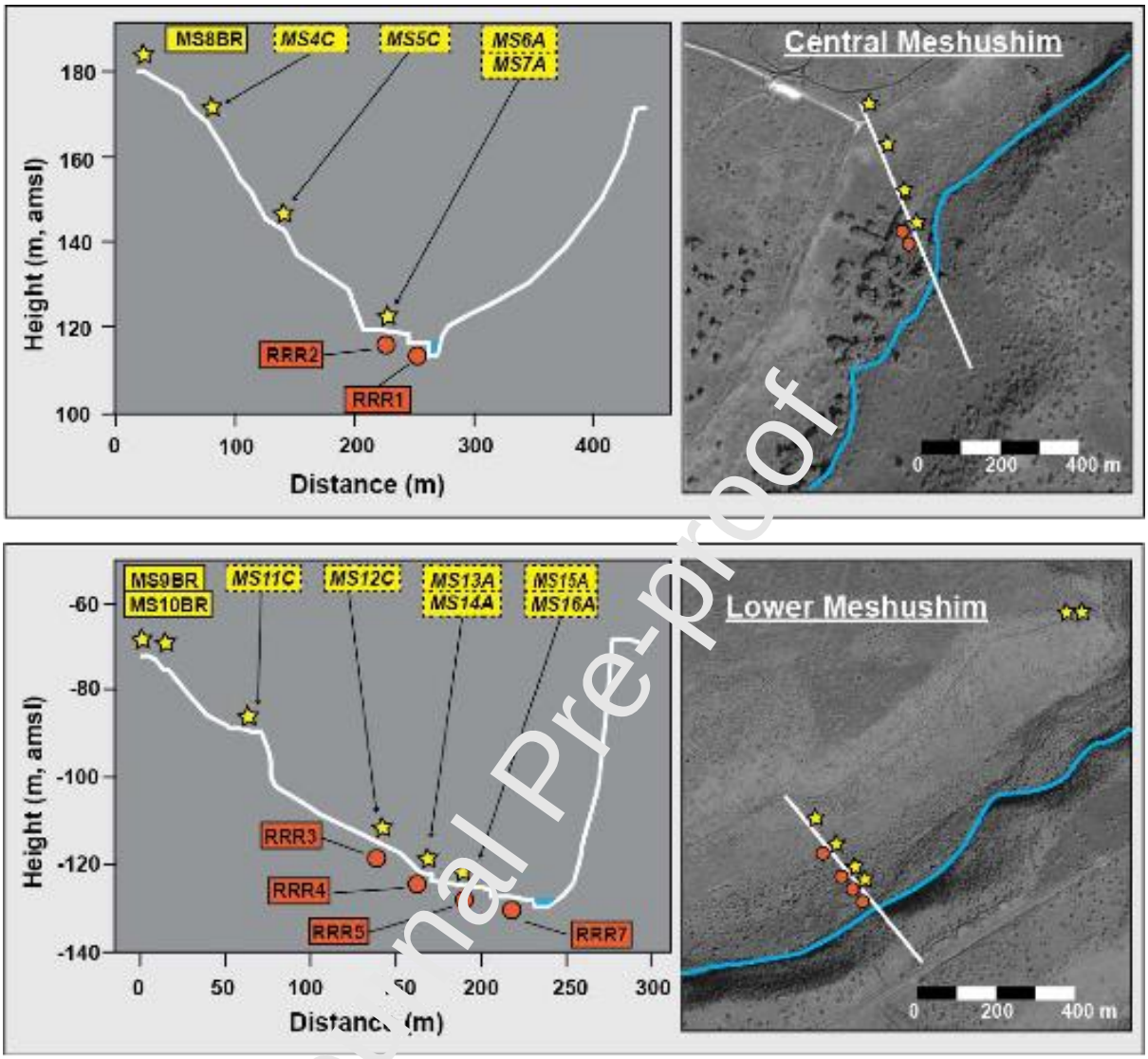

Fig. 4: Study cross sections in the Central and Lower Meshushim basin (for location see **Fig. 1**). OSL and ^{36}Cl sampling locations are marked along the cross section. Note that in the Lower Meshushim, two bedrock samples (MS9BR and MS10BR) were sampled a few hundred meters away (NE) of the main cross section, and are projected to main cross section in the left lower panel.

Table 1: Field description of cosmogenic nuclide samples collected in the Meshushim Stream

River section	Topographic location	Sample type	Sample name	Coordinates	Location in Fig. 3 cross-section.	Elevation amsl	Sample depth (cm)	Sample thickness (cm)	Density of sample or overlying material (g cm^{-3})	Scaling factor (spallation / muon-capture)
Upper Meshushim	Upper Plateau	Exposed bedrock	MS1BR	33°02'39.36'' N 35°43'32.52'' E	23.5	622	0	3	2.5	1.434 / 1.165
		Bedrock buried under soil	MS2BR	33°02'31.9'' N 35°43'18'' E	23	591	73	5	1.3	1.400 /1.148
		Bedrock buried under soil	MS3BR	33°02'31.9'' N 35°43'18'' E	23	591	162	3	1.3	1.400 / 1.148
Central Meshushim	Upper slope	Colluvial clasts	MS4C	32°58'28.2'' N 35°39'14.8'' E	13	177	0	2	2.5	1.004 / 0.941
	Mid slope	Colluvial clasts	MS5C	32°58'25.4'' N 35°39'16.8'' E	13	14[illegible]	0	2	2.5	0.973 / 0.924
	Upper terrace	Alluvial clasts	MS6A	32°58'21'' N 35°39'16.7'' E	13	126	0	2	2.5	0. 962 / 0.918
	Upper terrace	*Fine alluvial clasts*	*MS7A*	*32°58'21'' N 35°39'16.7'' E*	*13*	*126*	*0*	*0.1*	*2.5*	*1.16*
	Plateau above channel	Exposed bedrock	MS8BR	32°58'30.7'' N 35°39'13.2'' [illegible]	13	187	0	5	2.5	1.012 / 0.946
Lower Meshushim	Plateau above channel	Bedrock buried under soil	MS9BR	32°55'[illegible]7.2'' N 35°40'09.[illegible]'' E	6.7	169	21	7	1.3	0.997 / 0.937
		Exposed bedrock	MS10BR	32°55'27.2'' N 35°40'0[illegible].5'' E	6.7	174	0	3	2.5	1.001 / 0.939
	Mid slope	Colluvial clasts	MS11C	32°55'4'' N [illegible]°39'42.74'' E	5.7	118	0	2	2.5	0.954 / 0.914
	Lower slope	Colluvial clasts	MS[illegible]C	32°55'1.9'' N 35°39'44.34'' E	5.7	81	0	2	2.5	0.924 / 0.897
	Upper terrace	Alluvial clasts	MS13A	32°54'58.13'' N 35°39'46.69'' E	5.7	72	0	2	2.5	0.917 / 0.893
	Upper terrace	*Fine alluvial clasts*	*MS14A*	*32°54'58.13'' N 35°39'46.69'' E*	*5.7*	*72*	*0*	*0.1*	*2.5*	*1.31*
	Lower terrace	Alluvial clasts	MS15A	32°54'47.82'' N 35°39'22.63'' E	5.7	65	0	2	2.5	0.912 / 0.890
		Fine alluvial clasts	MS16A	32°54'47.82'' N 35°39'22.63'' E	5.7	65	0	0.1	2.5	0.912 / 0.890
Beit Tzeida valley	*Channel bank in delta*	*Alluvial clasts*	*MS17A*	*32°53'23.94'' N 35°37'17.17'' E*	*0.5*	*-200*	*0*	*2*	*2.5*	*1.29*
	Channel bank in delta	*Fine alluvial clasts*	*MS18A*	*32°53'23.94'' N 35°37'17.17'' E*	*0.5*	*-200*	*0*	*0.1*	*2.5*	*1.29*

Notes: 1) Bedrock samples comprise of in situ basalts. 2) Alluvial/ colluvial clast samples comprise of about 30-40 pieces of basalt clasts, about 1-3 cm in diameter. 3) Fine clasts samples include small (<1 cm) basalt clasts sieved and washed from soil samples. 4) Sediment samples used for basin wide erosion rates are shaded in grey and basin wide scaling factors are written in italic.

Table 2: Erosion rates calculated from ^{36}Cl concentration in samples from the Meshushim Stream

Basin region	Morphologic location	Sample type	Sample name	^{36}Cl (atoms/g)x10^4	Cl (ppm)	Denudation rate mm ka^{-1}
Upper Meshushim	Upper Plateau	Exposed bedrock	MS1BR	97.21±7.60	128.0±9.9	15.7±2.6
		Buried bedrock	MS2BR	16.37±1.29	79.6±4.1	124.3±22.6
		Buried bedrock	MS3BR	15.61±2.22	193.1±23.3	176.1±47.4
Central Meshushim	Upper slope	Colluvial clasts	MS4C	26.20±1.36	15.9±0.5	22.8±2.5
	Mid slope	Colluvial clasts	MS5C	23.15±1.28	19.2±0.6	26.7±3.0
	Upper terrace	Alluvial clasts	MS6A	24.22±1.40	25.7±0.9	27.2±3.1
	Upper terrace	*Fine alluvial clasts*	*MS7A*	*30.54±2.14*	*12.3±0.5*	*22.9±2.8*
	Plateau above channel	Exposed bedrock	MS8BR	32.9[illegible]1.60	4.6±0.2	14.2±1.6
Lower Meshushim	Plateau above channel	Buried bedrock	MS9BR	15.92±9.72	20.0±0.7	73.6±8.7
		Exposed bedrock	MS10BR	45.63±2.38	24.2±0.9	12.3±1.4
	Mid slope	Colluvial clasts	MS11C	6.00±0.47	18.1±0.6	119.9±14.5
	Lower slope	Colluvial clasts	MS12C	9.18±0.60	13.2±0.4	69.5±7.9
	Upper terrace	Alluvial clasts	MS13A	15.38±1.14	50.4±3.2	57.0±7.3
	Upper terrace	*Fine alluvial clasts*	*MS14A*	*9.58±1.19*	*26.4±0.9*	*265.6±42.3*
	Lower terrace	Alluvial clasts	MS15A	25.15±2.11	101.1±6.8	45.6±7.0
		Fine alluvial clasts	MS16A	26.48±2.72	177.9±6.4	67.9±12.3
Beit Tzeida Valley	*Near channel in delta*	*Alluvial clasts*	*MS17A*	*10.65±0.82*	*51.5±2.4*	*238.3±30.9*
	Near channel in delta	*Fine alluvial clasts*	*MS18A*	*4.90±0.49*	*11.7±0.4*	*520.3±70.9*

*Basin wide denudation rates are shaded in grey and are calculated using basin wide scaling factors as indicated in Table 1.

2.2 Optically stimulated luminescence (OSL)

Luminescence dating is used to estimate the last exposure of quartz and/or feldspar grains to sunlight during transport, and thus this method determines the time of sediment burial (Aitken, 1998). The method is widely used to date Quaternary deposits in alluvial terraces, colluvial deposits, and aeolian sediments such as loess and dunes (e.g., Matmon et al., 2016; Neagu et al., 2020; Faershtein et al., 2016). In fluvial environments, as grains are transported and buried intermittently, they go through cycles of OSL signal accumulation during burial and resetting when exposed to sunlight. However, sometimes when sediment is transported in water with high sediment load or during the night, the OSL signal may not be completely bleached and the OSL clock does not fully reset. Some grains would then contain a residual signal, which may lead to scatter in the dose distribution and, if not detected, age overestimation (Gliganic et al., 2017). In order to overcome this problem, we measured a relatively large number of small aliquots (~200 grains on a disc). For most samples, dose distribution was roughly normal and the central age model (CAM; Galbraith and Roberts, 2012) was used to obtain a representative equivalent dose (De) value. Nevertheless, distinct older outliers were removed, and by that, the influence of the allegedly old grains in the sample was avoided (Madsen and Murray 2009; Porat et al., 2012; Faershtein et al., 2016).

Former studies used OSL dating in the Golan Heights in archaeological sites (Freikman and Porat, 2017) or paleoseismology (Zilberman et al., 2000). However, this study is the first to use OSL dating in a fluvial system in this area. In this basaltic terrain, the source of all quartz grains is by long distance aeolian transport, brought by winds from the east and south (e.g., Foner et al., 2009), and it is well bleached at the time of deposition.

Seven OSL samples were collected in this study (**Figs 1,3,4; Table 3, Supplementary- Fig. 1**), five samples from terraces located from 2 m to about 20 m above stream level, one from a slope, and one sample from the delta of the Meshushim stream. Samples were collected from pits dug to 40-50 cm

depth, under a light-tight sheet to avoid recent exposure to sunlight, directly into a black light-tight plastic bag. A sediment subset was also collected for elemental analyses. Sample preparation, measurements, and analyses followed procedures described in Faershtein et al. (2016) and Davidovich et al. (2012) and were performed at the OSL laboratory, the Israel Geological Survey. Briefly, 75-125 µm quartz grains were extracted by wet-sieving, carbonates dissolved by 8% HCl, heavy minerals and feldspars removed by magnetic separation. The remaining feldspars were dissolved and quartz was etched with 40% HF, followed by soaking in 16% HCl overnight to dissolve any fluorides which may have precipitated. De values were measured on 2-mm aliquots using OSL signal and the single aliquot regenerative (SAR) protocol, with a preheat of 10 s at 260 ^{o}C, a test dose of ~4 Gy and a test dose preheat of 5 s at 200 ^{o}C. Dose rates were evaluated from the concentrations of the U, Th and K, measured on the subset sample. Water contents were estimated at 8% and cosmic dose calculated from current burial depth. Burial ages and errors were calculated using the CAM (Galbraith and Roberts, 2012).

Table 3: OSL data and ages from sediments collected in Nahal Meshushim

Basin region	Morphologic location	Lab code	Location in Fig. 3 cross-section.	Sample depth (m)	K (%)	U (ppm)	Th (ppm)	Ext. α (µGy/a)	Ext. β (µGy/a)	Ext. γ (µGy/a)	Cosmic (µGy/a)	Dose rate (µGy/a)	Aliquots	OD (%)	De (Gy)	Age (years)
Central Meshushim	Lower terrace	RRR1*	13	0.45	0.83	2.1	4.7	9	890	608	214	1721±60	40/42	52	0.85±0.06	490±40
	Upper terrace	RRR2*	13	0.45	0.68	1.4	5.7	7	734	547	214	1503±53	41/43	44	6.0±0.4	4000±290

Lower Meshushim	Lower slope	RRR3	5.7	0.4	0.39	1	5.7	7	496	436	219	1158±42	24/24	95	6.0±1.2	5100±1000
	Upper terrace	RRR4	5.7	0.4	0.64	1.2	5.9	8	694	529	219	1449±52	18/18	21	1.14±0.06	780±50
	Lower terrace	RRR5	5.7	0.4	0.91	1.8	4.7	8	909	594	219	1730±61	23/30	82	0.53±0.05	340±40
	Lowest terrace	RRR7	5.7	0.4	0.94	0.7	3.2	4	763	422	219	1448±49	19/24	100	1.3±0.3	940±210
Beit Tzeida valley	Near channel in delta	RRR6	0.5	0.5	0.81	0.9	3.2	5	697	409	210	1320±48	18/19	50	0.22±0.02	170±20

* Lab codes in Database are MSS-1 and MSS-2. For sample location see Fig. 3. ** Radial plots are shown in Supplementary Fig. 2

3.1 ^{36}Cl results

Overall, ^{36}Cl concentrations range between (4.90 ± 0.49) x10^4 atoms g^{-1} and (97.21 ± 7.60) x10^4 atoms g^{-1} (**Fig. 5; Table 2**). In exposed bedrock (n=3) the concentrations range between (97.21 ± 7.60) x10^4 atoms g^{-1} and (32.93 ± 1.60) x10^4 atoms g^{-1}. In soil covered bedrock (n=3) concentrations are very uniform and range between (15.61 ± 2.22) x10^4 atoms g^{-1} and (16.37 ± 1.29) x10^4 atoms g^{-1}. Colluvial samples collected along slopes (n=4) present concentrations that range between (6.00 ± 0.47) x10^4 atoms g^{-1} and (26.20 ± 1.36) x10^4 atoms g^{-1}. Coarse grained alluvial samples (n=4) collected on top of alluvial terraces present concentrations that range between (10.65 ± 0.82) x10^4 atoms g^{-1} and (25.15 ± 2.11) x10^4 atoms g^{-1}, while fine grained alluvial samples (n=4) present concentrations that range between (4.90 ± 0.49) x10^4 atoms g^{-1} and (30.54 ± 2.14) x10^4 atoms g^{-1}.

3.2. OSL results

All OSL ages are Holocene (**Table 3**). In the Central Meshushim, the upper terrace is 4000 years old while the lower terrace is only a few hundred years old. In the Lower Meshushim, the sediment at the foot of the slope, just above the upper terrace, has been buried for 5000 years. The upper terrace is ~800 years old while the lower terrace is ~300 years old. The sediment in the flood plain of the lower Meshushim (sample RRR7) has been buried for nearly 1000 years while that at the delta, less than 200 years. The young ages demonstrate the lack of any long term storage of sediments in the Meshushim drainage basin.

4. Discussion

4.1. ^{36}Cl

4.1.1 ^{36}Cl concentrations

We discuss concentrations since they serve as isotopic signatures for the source of sediment in the stream. As we follow the drainage system from its upper reaches down-stream we see that exposed bedrock (samples MS1BR, MS8BR, MS19BR) yielded the highest ^{36}Cl concentrations relative to all other samples in the basin (**Fig. 5**). This is true also in the middle and lower parts of the basin, in spite of the decrease in elevation. In contrast, soil covered bedrock yielded significantly lower concentrations, regardless of elevation (-20 to 600 m amsl) and local precipitation levels (400-1000 mm/year) (**Fig. 6**). The difference between exposed and covered bedrock means that bedrock outcrops are not covered and exposed very frequently, otherwise concentrations among these two types of samples would have been similar. A rough estimation of the time of continuous cover of buried bedrock and continuous exposure of exposed bedrock is given by the differences in ^{36}Cl concentrations between adjacent exposed and buried bedrock. In the Upper Meshushim, this difference is ~$80x10^4$ atoms g^{-1}. At this site, the difference in production rates between exposed and

buried bedrock (due to soil cover of 73 and 162 cm) ranges between 130-200 atoms g^{-1} yr^{-1}. At these rates, the time it would take to accumulate the difference in concentrations ranges between 4-6 ky. In the lower Meshushim, the difference is ~30x10^4 atoms g^{-1}. Here, the difference in production rates between adjacent exposed and buried bedrock (due to soil cover of 21 cm) is 100 atoms g^{-1} yr^{-1}. At this rate, the time it would take to accumulate the difference in concentrations is ~3 ky. Although these calculations provide only a rough estimate of the coverage time, it seems that in the Golan Heights, in general, and in the Meshushim drainage system, in particular, soil cover is only a few thousand years old. In terms of soil formation processes and their effect on cosmogenic isotope accumulation, there are two possibilities: (a) accumulation-removal cycles of soil take only several thousands of years; or (b) a unique, and singular soil stripping event occurred in the Golan Heights during the middle Holocene, and soils are just beginning to re-accumulate. Since no stripping event has been recorded in the Golan Heights, the first option seems more reasonable.

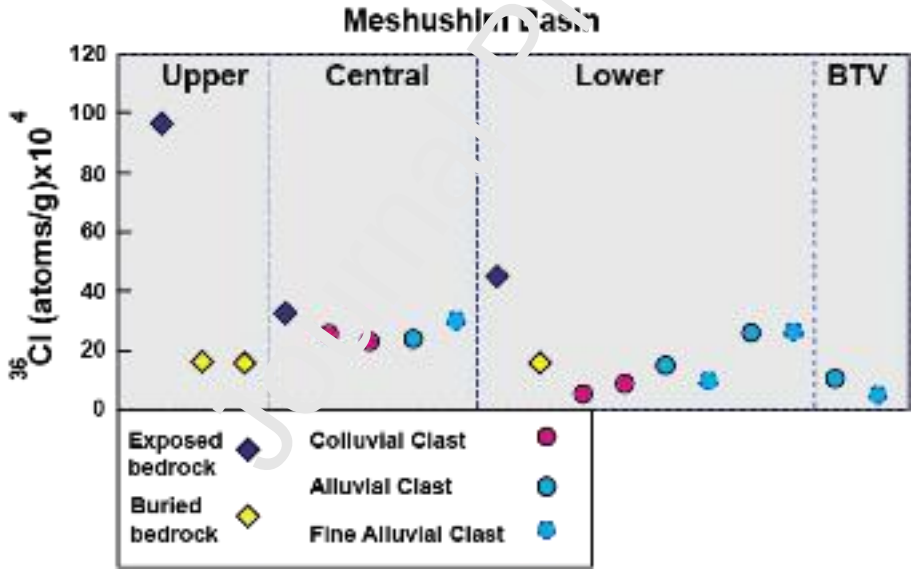

Fig. 5: ^{36}Cl concentrations (atoms/g) X 10^4 for the various types of samples.

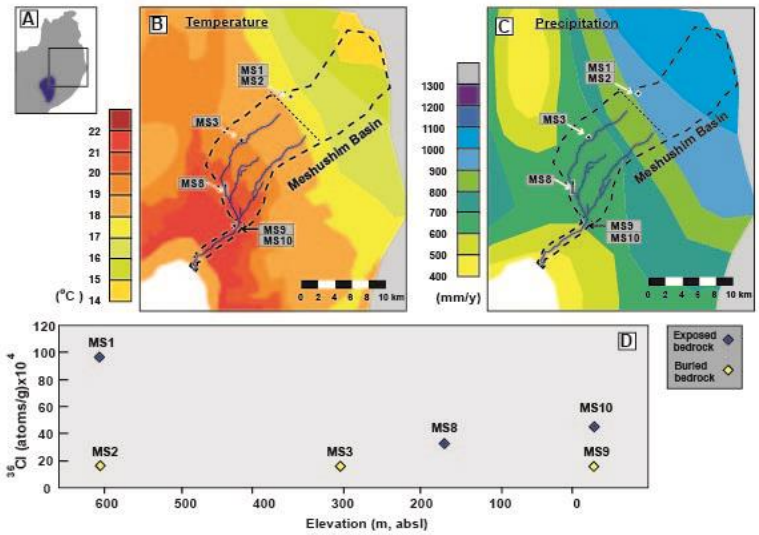

Fig. 6: (A) Location of study area in northern Israel. (B) Average annual temperature map (for the years 1995-2011). (C) Average annual precipitation (modified from Halfon and Yosef, 2021). The Meshushim Basin and location of bedrock samples is indicated by white arrows in B and C . (D) Elevation vs. ^{36}Cl concentrations (atoms/g) X 10^4 for bedrock samples.

When comparing the measured concentrations in bedrock to all other samples in the drainage system it is apparent that concentrations measured in buried bedrock are similar to those measured in alluvial and colluvial sediment samples, while those measured in exposed bedrock are generally higher (**Fig. 5**). This points to the fact that the weathering of buried rock, and the production of basalt clasts at the bedrock-soil interface, is a major source for sediment in the drainage system, while exposed bedrock is a minor source for sediment. For example: in the central part of the stream (Central Meshushim), ^{36}Cl concentrations of 23x10^4-26x10^4 atoms/gram were measured in the colluvial clasts samples (samples MS4C and MS5C, **Table 2**). In contrast, in the Upper and Central Meshushim, ^{36}Cl concentrations of 32x10^4- 97x10^4 atoms/gram were measured in the exposed bedrock samples and 15x10^4- 16x10^4 atoms/gram in the buried bedrock samples. Considering all these measurements together, it seems that ^{36}Cl concentrations in clasts on slopes is the result of mixture of clasts derived from buried bedrock (50-90%) and clasts derived from exposed bedrock (10-50%). In the Central Meshushim, this trend still holds, although not as pronounced as in the

Upper Meshushim. Here, the ^{36}Cl concertation measured in exposed bedrock, although still much higher than concentrations measured in buried rock, is closer to the concentrations measured down the slope within the canyon and on top of the alluvial terraces. This means that in this section of the basin, exposed bedrock could be a greater contributor of sediment to the slopes and the river bed.

Five sediment samples in the Lower Meshushim and the BTV yielded very low concentrations ($\leq 11 \times 10^4$ atoms g^{-1}) (**Table 2; Fig. 5**). The source for such sediment cannot be explained by weathering of soil-covered bedrock. However, landslides and earth slides may contribute to the river system sediment with very low cosmogenic isotope concentrations as discussed below. Along the slopes of the Golan Heights' canyons (including the Meshushim basin), exposed sequences of alternating basalt flows and paleosols provide a setting which is prone to sliding. In fact, currently, most of the sediment movement on the slopes occurs by sliding, on the range of a few meters thick sections, generally during the winter and spring (Inbar and Even-Nir, 1989; Ankori, 2014).

Comparing between ^{36}Cl concentrations of colluvial material in the Central Meshushim and the Lower Meshushim (**Fig. 7**), shows significant differences between these two locations. In the Central Meshushim, mid and upper slope samples yielded concentrations of $23.15 \pm 1.28 \times 10^4$ atoms g^{-1} and $26.2 \pm 1.36 \times 10^4$ atoms g^{-1}, respectively. These concentrations can be easily explained by material, mostly derived from weathering of soil covered bedrock (e.g., sample MS8BR**; Table 2; Fig. 4-7**), with a small addition of weathering products from exposed bedrock. Similarly, concentrations of $24.22 \pm 1.40 \times 10^4$ atoms g^{-1} and $30.54 \pm 2.14 \times 10^4$ atoms g^{-1} were measured in the coarse and fine fractions, respectively, of the sediment on the upper alluvial terrace in the Central Meshushim. Again, these concentrations can be easily explained by mixing of material derived from sub-surface bedrock weathering, and varying contributions of weathering products from exposed bedrock.

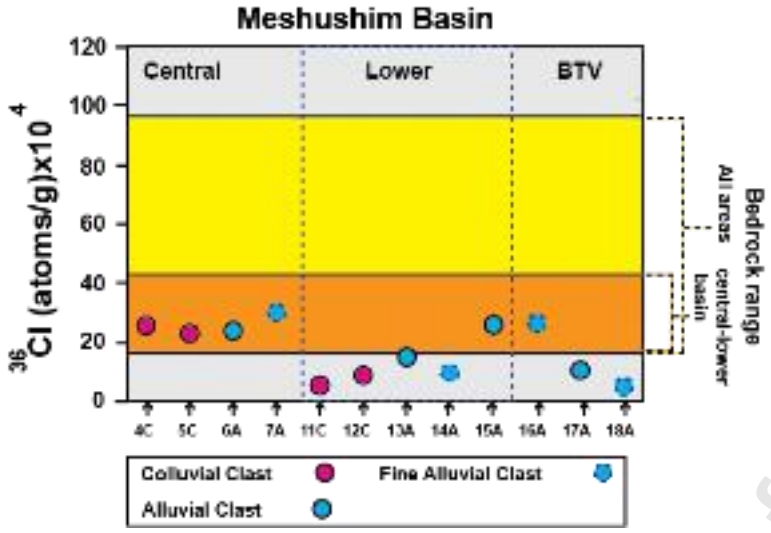

Fig. 7: ^{36}Cl concentrations (atoms/g) X 10^{4}of colluvial and alluvial samples vs. the ranges of bedrock samples from the Central and Lower Meshushim (orange background) and the entire basin (yellow+ orange background).

In contrast, in the Lower Meshushim, mid and lower slope samples yielded concentrations of 6.0±0.47 x10^{4} atoms g^{-1} and 9.2±0.60 x10^{4} atoms g^{-1}, respectively (**Fig. 7**). As noted above, these concentrations cannot be explained by bedrock weathering (exposed or buried). Sediment on this slope must have been supplied by mass wasting from deeply shielded rock (not to be confused with shallow soil covered samples in this study), as is also indicated by field observations. This contribution of such sediment from the slope is also reflected in the concentrations measured in the alluvial terrace at the base of the slope. Here, concentrations of 15.38±1.14 x10^{4} atoms g^{-1} and 9.58±1.19 x10^{4} atoms g^{-1} were measured in the coarse and fine fractions of the sediment, respectively, on the upper alluvial terrace in the lower Meshushim. It should be noted here that a fraction (7-215 x 10^{3} atoms) of the measured ^{36}Cl concentration may have accumulated during residence of the sediment on the terrace. The post deposition production of ^{36}Cl enhances the dominant role of sediment supplied from shielded rock is also manifested by the measured ^{36}Cl concentrations in sediment at the outlet of the Meshushim Stream, at the BTV (**Fig. 1**). Here,

concentrations range between $5x10^4$ and $11x10^4$ atoms/g^{-1}, clearly indicating that most of the sediment that eventually reaches the base level at the shores of the Sea of Galilee was generated through mass wasting.

It should be noticed that the BTV samples, collected from the delta of the Meshushim basin into the Sea of Galilee, might be influenced by the Jordan river (i.e., these samples may include different sources beside the Meshushim stream itself). However, Inbar and Even-Nir (1989) and Ankori (2014) found that most of the sediment in the Jordan river is also derived from slides along the lower stream channel. These slides are particularly active during and right after medium to large floods that erode the banks. Although only the Meshushim Stream channel was studied in this research, a similar process seems to be operating throughout other Golan Heights drainage systems.

4.1.2 Denudation rates

Assuming steady state erosion, bedrock denudation rates calculated from the concentrations of cosmogenic isotopes are averaged over the time it takes to remove an overburden thickness of approximately one attenuation length, generally about 0.7 m of rock. This sets the temporal framework relevant for the results presented above. Sample MS10 yields the slowest bedrock erosion rate calculated in this study (12.3±1.4 mm/ka). At this rate, ~70 cm of rock is removed within ~60 ka years. Thus, the denudation rate calculated from the ^{36}Cl concentration in sample MS10 is averaged over the current inter-glacial period, the Holocene, and most of the Late Pleistocene glacial period.

Denudation rates are calculated for all samples (**Table 2**). However, they are meaningful only for two types of samples:

1. ***Site specific denudation***: Site specific denudation is calculated from the ^{36}Cl measured concentrations in bedrock samples. In the Meshushim basin, these rates, calculated from

bedrock samples, range from 12.3±1.4 mm/ka in exposed bedrock to 124.3±22.6 mm/ka in buried bedrock (**Table 2; Fig. 5**).

In Upper Meshushim, the buried bedrock denudes at rates 9 to 11 times faster than exposed bedrock (15.7±2.6 mm ka^{-1} in exposed bedrock and 124.3±22.6 and 176.1±47.4 mm ka^{-1} in buried bedrock). In lower Meshushim, the difference is slightly smaller, 6 times faster (73.6±8.7 mm ka^{-1} in buried bedrock and 12.3±1.4 mm ka^{-1} in exposed bedrock). The reason for the differences in denudation rates is most likely the significant chemical weathering that occurs at the bedrock-soil interface, where moisture residence time is long and biological activity accelerates rock and mineral decomposition. Furthermore, in the Meshushim basin, there is no significant freeze-thaw process that can lead to higher weathering rates of exposed rocks.

Overall, bedrock denudation rates are similar among the various parts of the Meshushim stream (Upper, Central, Lower, and BTV), in spite of 600 mm/y differences in annual precipitation (**Fig. 7**), and up to 10 C° in annual average temperature from the BTV and upstream to the Upper Meshushim. It is apparent that the current precipitation-temperature gradients are not sufficient to promote significant differences in denudation rates.

2. ***Weighted, basin wide average denudation rates***: These are estimated from the concentration of ^{36}Cl in alluvial material (e.g., Bierman and Steig, 1996; Granger et al, 1997; Matmon et al., 2003). Calculating basin-wide erosion rates is based on two assumptions: (1) the clasts (which are amalgamated into one sample) are derived uniformly from the entire basin, and (2) transport is instantaneous, therefore, measured ^{36}Cl concentrations represents average bedrock erosion rate and not ^{36}Cl that accumulated during transport. Basin- wide erosion rates were calculated from 4 alluvial sediment samples in the basin: (1) the terrace in central Meshushim (sample MS7A), (2) the terrace in lower Meshushim (sample MS14A), and (3) the BTV delta (samples MS17A and MS18A).

All results represent average basin wide erosion upstream of the sampling location. Thus, (a) the terrace in central Meshushim represents the erosion rate of the upper part of the Central Meshushim and the Upper Meshushim at the time of terrace deposition, (b) the terrace in Lower Meshushim represents the erosion of the Lower, Central and Upper Meshushim at the time of terrace deposition, and (c) the delta represents the erosion rate in the entire basin. Only the BTV samples (samples MS17A and MS18A) represent basin wide erosion that is averaged to the present. The other two samples represent basin wide erosion rates that are averaged only to the time the sediment was deposited (determined from the OSL measurements): 4000±290 yrs (Sample RRR2; **Table 3**) for the upper terrace in the Central Meshushim and 780±50 yrs (Sample RRR4; **Table 3**) for the upper terrace in the Lower Meshushim. It should be noticed that since a fraction of the measured ^{36}Cl concentrations in alluvial terrace sediments may have been accumulated after deposition, basin wide erosion rates may in fact be slightly faster than calculated.

The Central Meshushim sample (MS7A) yielded a basin wide erosion rate of 22.9±2.8 mm/ka (**Tables 2, 4; Fig. 8A, B**). This rate correlates well with the calculated denudation rates for buried bedrock in the Upper and Central Meshushim. Thus, the averages basin wide denudation is controlled by bedrock erosion. However, this rate is an order of magnitude slower than the rates calculated in the Lower Meshushim (265.6±42.3 mm/ka; MS14A) and BTV (238.3±30.9 mm/ka; MS17A; 520.3±70.9 mm/ka; MS18A) (**Tables 2,4; Fig. 8A, B**). The dramatic increase in basin wide erosion between the higher parts of the Meshushim basin and the lower parts, correlates well with the dramatic decrease in ^{36}Cl concentrations as measured in colluvial material. This difference could, therefore, be the result of steady bedrock erosion in the upper part of the system as opposed to the dominance of mass wasting in sediment production and transport along the lower part of the drainage system.

Figure 8C shows a thalweg vs. ridge profile from the base level point at the BTV and 20 km upstream within the Meshushim Stream. It is evident that the lower part of Central Meshushim has the greatest relief, a situation that would promote land sliding due to increased exposure of basaltic flows and the paleosols between them, thus, explaining the low dosed material on the slopes and the high basin-scale denudation rates calculated for samples 14A, 17A and 18A.

While, as discussed above, basin-scale denudation rates were calculated for samples ranging in age over a few thousand years to a few hundred years, the basin wide denudation rate pattern correlates with the geomorphological profile and thus does not necessarily represent temporal evolution of denudation rates in the Meshushim basin.

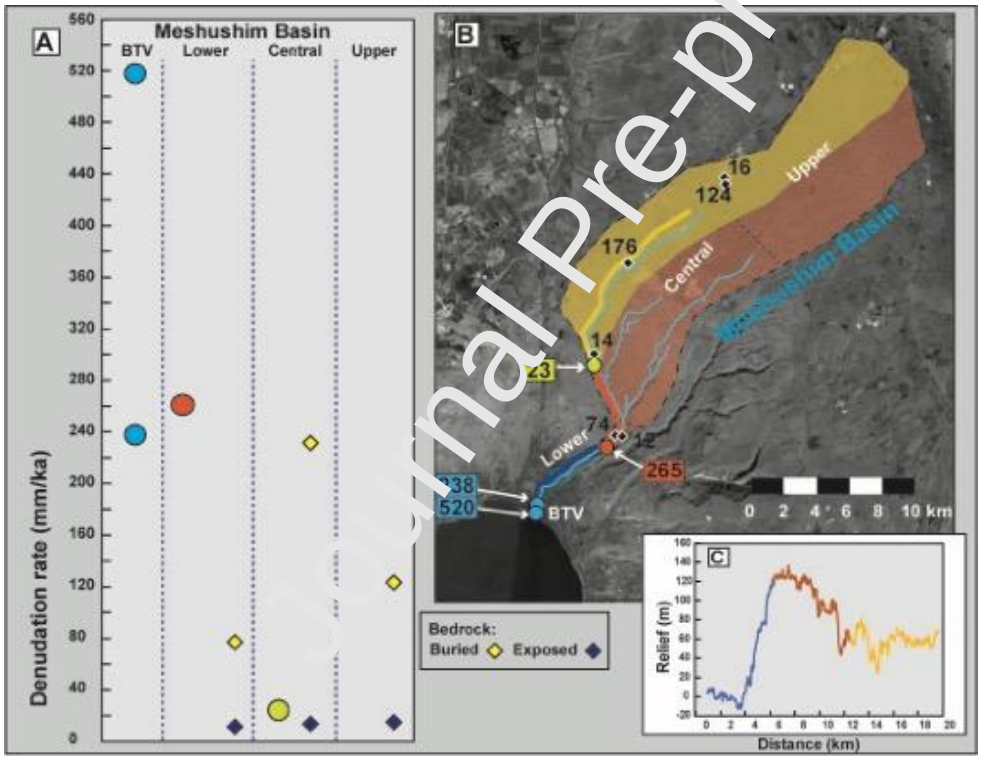

Fig. 8: (A) Denudation rates (mm/ka) for bedrock samples and calculated basin -wide denudation rates for alluvial samples (shown on map in B). (B) location of bedrock samples and associated specific denudation rates, as well as with basin-wide denudation rates for the alluvial samples covering sub- to entire basin-scale, by colour. (C) Thalweg vs. ridge profile relief over 20 km section from the basin base level upstream the Meshushim Stream. Location of section is marked in (B).

Site specific denudation rates calculated for the Meshushim drainage are within the range of rates calculated for different lithologies over climatic gradients from hyper arid to Mediterranean along the margins of the DSR (**Fig. 9**). However, of the four basin wide denudation rates calculated in this study, three are above 200 mm/ky with the highest being 520 mm/ky. These are exceptionally high relative to all other basin wide denudation rates measured along the Dead Sea rift and may be the result of the unique setting of exposed basalt flows with intercalated paleosols.

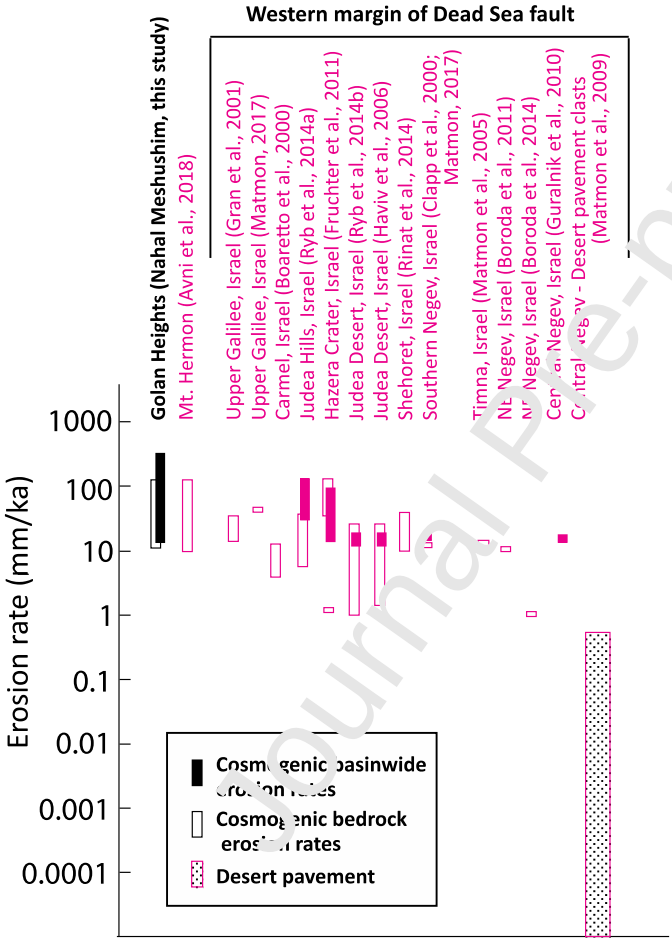

Fig. 9: Compilation of erosion rates calculated from cosmogenic concentrations in bedrock, boulder, and sediment samples from selected studies along the DSR. Apart from the Paran Plains, erosion rate measurements along the western margin of the Dead Sea fault range between 1 and 100 mm/ka. Apparently, the climatic and tectonic conditions along the western Margin of the Dead Sea fault are not extreme enough to

result in extreme, atypical high or low erosion rates. Erosion rates in the Golan Heights are within the typical range for the Dead Sea Rift margins.

4.2 Sediment storage and sediment yield

In the Meshushim drainage system, sediment is stored in several geomorphic locations: 1) soil pockets and soil blankets on the upper plateau, 2) colluvial material on slopes, and 3) alluvial terraces. As shown in section 4.1, differences in ^{36}Cl concentrations between exposed and covered bedrock suggest soil residence time of only several thousands of years. Similarly, OSL ages of sediments stored in alluvial terraces and at the base of slopes, point to storage on the order of only a few thousands to few hundreds of years (**Table 3**). Nowhere in the Meshushim drainage system did we find evidence for long-term storage of sediment or soil of more than a few thousands of years.

Basin wide denudation rates calculated from ^{36}Cl concentrations measured in samples MS7A, MS14A, MS17A and MS18A are used to calculate the sediment yield (**Table 4**). We also compared sediment yield results at BTV with sediment yield calculations that were done using other methods. Basin wide denudation rates calculated from ^{36}Cl concentrations measured in samples MS17A and MS18A, are 238.3±30.9 and 520.3±70.9 mm/ky, respectively (**Table 4**). Based on the fact that residence time of sediment storage in the Meshushim is on the order of only a few thousands of years at the most, we can assume that basin wide erosion translates well into a long-term sediment yield average value. Therefore, using the calculated basin-wide erosion rates, we calculate the sediment yield into BTV to be 640 ton/km^2/yr for the coarse alluvial material (sample MS17A) and 1400 ton/km^2/yr for the fine alluvial material (sample MS18A). The latter estimate for fine alluvial material, is two orders of magnitude higher than recent multi annual (1972-2015; 24 ton/km^2/y) sediment loads calculated from total suspended solids (TSS) (Meshushim TSS data from Israeli Water Authority monitoring program via the Mekorot water company), measured at the mouth of the Meshushim at the BTV. It is also much higher than values provided by other studies of the present-

day total sediment yield (Inbar, 1992; Grodek, 1994; Bergman et al., 2018, 2021) all of which are <100 ton/km^2/y. Notably, both our estimates from the BTV (coarse and fine material) are higher, but on the same scale as the controversial total annual sediment load of 630 ton/km^2 estimated by Inbar and Schick (1979) for 1969. Our estimated sediment yield calculated from fine alluvial material sample in the BTV is several times higher than TSS calculated loads for1992 (123 ton/km^2/y). It is worth mentioning that in the recent record both years, 1969 and 1992, were characterized by unusually high precipitation and flooding in the Meshushim basin, thus extremely high sediment loads are to be expected for these years.

We assume that the present yield measurements represent the very late part of the Holocene, while the yields calculated from the basin wide erosion rates (based on cosmogenic isotopes) represent the average of earlier parts of the Holocene and up to the last ~45-60 ka (as discussed above in relation to the duration over which cosmogenic isotope-based erosion rates can be averaged). Therefore, the cosmogenic yield values average over the present interglacial period and to a minor extent into the last glacial. The comparison between the results of this study and the present yield measurements suggest temporal changes in denudation rates, with higher denudation rates and sediment yields during most of the Holocene relative to present denudation and sediment yield. Previous studies (Grodek, 1994) indicated that the presence of very large boulders at the delta of the Meshushim stream indicated that the stream must have had past high transport capacities during larger flow events. This is interpreted in the context of our results to reflect more dominant denudation and sediment yields, including large distance transport of boulders during the earlier part of the Holocene, or earlier. This conclusion is partially concurrent with the Late Pleistocene glacial to Holocene interglacial climate record in this region which suggests 1.5 - 2 times more precipitation than today (Ryb et al., 2014a, b; Enzel et al., 2008), although our estimates that the present day denudation and sediment yields are lower than most of the Holocene has currently no support from other studies in this region.

Table 4. Sediment yields in the Meshushim basin

	Erosion rate (mm/ky)	Area size (km²)	Rock density (g/cm^3)	Sediment yield ($Tons/km^2/yr$)
Above central Meshushim (MS7A)	22.9±2.8	128	2.7	62
Above lower Meshushim (MS14A)	265.6±42.3	153	2.7	718
Entire basin (MS17A) (MS18A)	238.3±30.9 520.3±70.9	157	2.7	642 1404

5. Conclusions

- Denudation rates calculated for bedrock basalts differ between exposed bedrock (12.3±1.4 mm/ka) and soil covered bedrock (176.1±47.4 mm/ka), this being consistent over the basin despite notable variations in average annual temperature and precipitation. This means that chemical weathering at bedrock-soil interface is a significant factor controlling erosion.
- Differences in ^{36}Cl concentrations between exposed and covered bedrock suggest soil residence time of only several thousands of years. Similarly, OSL ages of sediments stored in terraces range between 170±20 and 4000±290 years. Nowhere in the Meshushim drainage system did we find evidence for storage of sediment or soil longer than a few thousands of years.
- Sub-surface weathering of basalts seems to be the major source for sediments in upper and central segments of the basin, as evidenced by similar ^{36}Cl concentrations. However, low dosed ^{36}Cl in the lower parts of the basin indicate involvement of landslides which instantaneously supply previously shielded sediment into the river. This conclusion correlates well with the observation that the highest relief (difference between thalweg and

top of ridge) which exposes the most paleosol-basalt flow layers, is located along the lower Meshushim.

- Site specific, as well as basin wide, denudation rates calculated for the Meshushim drainage basin are within the range of rates calculated for different lithologies over climatic gradients from hyper arid to Mediterranean along the margins of the Dead Sea Rift.
- The Upper Meshushim and the upper part of the Central Meshushim are characterized by basin-wide denudation rates concurrent with site-specific denudation rates as measured from bedrock samples, and fit well with moderate to low relief (**Fig. 8**). In contrast, basin-wide denudation rates in the lower part of the central Meshushim, and downstream to the basin base-level at the BTV increase dramatically, do not correlate with site specific rates, but are concurrent with high relief which allows the increasing role of landslides.
- The high sediment yields calculated from this work suggest temporal changes in denudation rates over the Holocene and possibly over earlier periods, during the last ~60 ka, with higher past denudation rates and sediment yield. In part these results can be related to the Late Pleistocene glacial to Holocene interglacial climate record in this region which suggests significantly more precipitation than today.

Acknowledgements

This study was funded by the kind support of the Israeli Ministry of Science, Technology and Space grant # **2015-6-93**. The authors wish to thank E. Ben-Tzur for his support preparation of figures. Y.Be'e'ri-Shlevin wishes to dedicate this paper to I. Sirkin.

References

Aitken, M.J., 1998. An Introduction to Optical Dating. The Dating of Quaternary Sediments by the Use of Photon-Stimulated Luminescence. xi + 267 pp. Oxford, New York, Tokyo, Oxford University Press.

Anders, A.M., Roe, G.H., Hallet, B., Montgomery, D.R., Finnegan, N.J., Putkonen, J., 2006. Spatial patterns of precipitation and topography in the Himalaya, in Willett, S.D., et al., eds., Tectonics, climate and landscape evolution: Geological Society of America Special Paper 398, p. 39–53.

Alcalá-Reygosa, J., Palacios, D., Schimmelpfennig, I., Vázquez-Selem, L., García-Sancho, L., Franco-Ramos, O., Villanueva, J., Juan Zamorano J., Keddadouche, K., 2018. Dating late Holocene lava flows in Pico de Orizaba (Mexico) by means of in situ-produced cosmogenic ^{36}Cl, lichenometry and dendrochronology. Quat. Geochronol. 47, 93-106.

Ankori, E., 2014. Loads, Sources and Properties of the Suspended Sediments Entering into Lake Kinneret from the Jordan River. Unpublished M.A. thesis, University of Haifa [Hebrew, English abstract].

Arnold, M., Aumaître, G., Bourlès, D.L., Keddadouche, K., Braucher, R., Finkel, R.C., Nottoli, E., Benedetti, L., Merchel S., 2013. The French accelerator mass spectrometry facility ASTER after 4 years: Status and recent developments on 36Cl and 129I. Nuclear Instruments and Methods in Physics Research Section B: Beam Interactions with Materials and Atoms 294, 24-28. ISSN 0168-583X. https://doi.org/10.1016/j.nimb.2012.01.049.

Avni, S., Haviv, I., Matmon, A., Benedetti, L., ASTER Team., 2018. Patterns and rates of 10^3-10^5 yr denudation in carbonate terrains under sub-humid to sub-alpine climatic gradient, Mount Hermon, Israel. Geol. Soc. Am. Bull. https://doi.org/10.1130/B31973.1.

Barreto, H.N., Varajão, C.A., Braucher, R., Bourlès, D.L., Salgado, A.A., Varajão, A.F., 2013. Denudation rates of the Southern Espinhaço Range, Minas Gerais, Brazil, determined by in situ-produced cosmogenic beryllium-10. Geomorphology, 191, 1-13.

Behar, N., Shaar, R., Tauxe, L., Asefaw, H., Ebert, Y., Heimann, A., Koppers, A.A.P., Ron, H., 2019. Paleomagnetism and paleosecular variations from the Plio-Pleistocene Golan Heights volcanic plateau. Israel: Geochemistry, Geophysics, Geosystems. https://doi.org/10.1029/2019GC008479

Ben-Avraham, Z., Brink, U., Bell, R., Reznikov, M., 1996. Gravity field over the Sea of Galilee : Evidence for a composite basin along a transform fault J. Geophys. Res. 101 (B1), 533-544.

Benedetti, L., Finkel, R., Papanastassiou, D., King, G., Armijo, R., Ryerson, F., Farber, D., Flerit, F., 2002. Post-glacial slip history of the Sparta fault (Greece) determined by ^{36}Cl cosmogenic dating: Evidence for non-periodic earthquakes. Geophys. Res. Lett. 29(8), 87-1.

Benedetti, L., Manighetti, I., Gaudemer, Y., Finkel, R., Malavieille, J., Pou, K., Arnold, M., Aumaître, G., Bourlès, D., Keddadouche, K., 2013. Earthquake synchrony and clustering on Fucino faults (Central Italy) as revealed from in situ ^{36}Cl exposure dating. J. Geophys. Res., Solid Earth 118(9), 4948-4974.

Benedetti L., Guillou V., ASTER Team., 2016. Weathering-limited hillslope evolution in carbonate landscapes. Earth Planet. Sci. Lett. 446, 10-20.

Bergman, N., Greenbaum, N., Be'eri-Shlevin, Y., Glassman, H., Nusboim, S., 2018. Suspended and bedload sediment transport in a basaltic gravel-bed stream, Nahal Meshushim, Israel. The 49th Geomorphology Binghamton Symposium, October 2018, University of Syracuse, Syracuse, New York, USA.

Bergman, N., Greenbaum, N., Koren, L., Glassman, H., 2021. Bedload transport and channel morphology during an extreme flood event, Nahal Meshushim, Central Golan Heights and NE Sea of Galilee. Geological Society of America (GSA) Annual Meeting October 2021, Portland, Oregon, USA.

Bierman, P.R., 1994. Using in situ produced cosmogenic isotopes to estimate rates of landscape evolution: A review from the geomorphic perspective. J. Geophys. Res. Solid Earth 99(B7), 13885-13896.

Bierman, P., Steig, E.J., 1996. Estimating rates of denudation using cosmogenic isotope abundances in sediment. Earth Surf. Process. Landf. 21 (2), 125-139.

Bierman, P., Gillespie, A., Caffee, M., Elmore, D., 1995. Estimating erosion rates and exposure ages with ^{36}Cl produced by neutron activation. Geochim. Cosmochim. Acta. 59(18), 3779-3798.

Bierman, P.R., Coppersmith, R., Hanson, K., Neveling, J., Portenga, E.W., Rood, D.H., 2014. A cosmogenic view of erosion, relief generation, and the age of faulting in southern Africa. GSA Today. 24(9), 4-11.

Boaretto, E., Berkovits, D., Hass, M., Hui, S., Kaufman, A., Paul, M., Weiner, S., 2000. Dating of prehistoric caves sediments and flints using 10Be and 26Al in quartz from Tabun Cave (Israel): Progress report. Nuclear Instruments and Methods in Physics Research Section B: Beam Interactions with Materials and Atoms. 172. 767-771. 10.1016/S0168-583X(00)00349-9.

Boroda, R., Amit, R., Matmon, A., Finkel, R., Porat, N., Enzel, Y., Eyal, Y., ASTER Team, 2011. Quaternary-scale evolution of sequences of talus flatirons in the hyperarid Negev. Geomorphology 127 (1-2), 41-52.

Boroda, R., Matmon, A., Amit, R., Haviv, I., Arnold, M., Aumaître, G., Bourlès, D.L., Keddadouche, K., Eyal, Y., Enzel, Y., 2014. Evolution and degradation of flat-top mesas in the hyper-arid Negev, Israel revealed from 10Be cosmogenic nuclides. Earth Surf. Process. Landf. 39 (12), 1611-1621.

Bull, W.B., 1991. Geomorphic Responses to Climate Change. Oxford University Press, Oxford.

Burbank, D., Leland, J., Fielding, E., Anderson, R.S., Brozovic, N., Reid, M.R., Duncan C., 1996. Bedrock incision, rock uplift and threshold hillslopes in the northwestern Himalayas. Nature 379, 505–510. https://doi.org/10.1038/379505a0.

Charton, J., Schimmelpfennig, I., Jomelli, V., Delpech, G., Blard, P-H., Braucher, R., Verfaillie, D., Favier, V., Rinterknecht, V., Goosse, H., Crosta, X., Chassiot, L., Martin, L., Guillaume, D., Legentil, C., ASTER Team, 2022. New cosmogenic nuclide constraints on Late Glacial and Holocene glacier fluctuations in the sub-Antarctic Indian Ocean (Kerguelen Islands, 49°S). Quat. Sci. Rev. 283, 107461. https://doi.org/10.1016/j.quascirev.2022.107461.

Clapp, E.M., Bierman, P.R., Schick, A.P., Lekach, J., Enzel, Y., and Caffee, M., 2000. Sediment yield exceeds sediment production in arid region drainage basins. Geology 28 (11), 995–998. doi: 10.1130/0091-7613 (2000 28<995:SYESPI>2.0.CO;2.

Davidovich, U., Porat, N., Gadot, Y., Avni, Y., 2012. Archaeological investigations and OSL dating of terraces at Ramat Rahel, Israel. J. Field Archaeol. 37(3), 192-208.

Di Biase, R.A., Whipple K.X., 2011. The influence of erosion thresholds and runoff variability on the relationships among topography, climate, and erosion rate. J. Geophys. Res. Atmos. 116(F4), 06- DOI:10.1029/2011JF002095

Dunai, T.J., 2010. Cosmogenic nuclides: principles, concepts and applications in the earth surface sciences. Cambridge University Press.

Enzel, Y., Amit, R., Dayan, U., Crouvi, O., Kahana, R., Ziv, B., Sharon, D., 2008. The climatic and physiographic controls of the eastern Mediterranean over the late Pleistocene climates in the southern Levant and its neighboring deserts. Glob. Planet. Change. 60 (3–4), 165-192. doi: 10.1016 /j.gloplacha.2007 .02 .003.

Faershtein, G., Porat, N., Avni, Y., Matmon, A., 2016. Aggradation–incision transition in arid environments at the end of the Pleistocene: An example from the Negev Highlands, southern Israel. Geomorphology 253, 289-304.

Fernández-Fernández, J.M., Palacios, D., Andrés, N., Schimmelpfennig, I., Brynjólfsson, S., Sancho, L.G., Zamorano, J.J., Heiðmarsson, S., Sæmundsson, Þ., ASTER Team, 2019. A multi-proxy approach to Late Holocene fluctuations of Tungnahryggsjökull glaciers in the Tröllaskagi peninsula (northern Iceland). Sci. Total Envriron. 664, 499-517. https://doi.org/10.1016/j.scitotenv.2019.01.364.

Fink, D., Vogt, S., Hotchkis, M., 2000. Cross-sections for 36Cl from Ti at Ep¼35–150MeV: applications to in-situ exposure dating. Nucl. Instrum. Methods Phys. Res. B 172, 861866.

Foner, H.A., Ganor, E., Gravenhorst, G., 2009. The chemical composition and sources of the bulk deposition on Lake. Kinneret (The Sea of Galilee), Israel. J. Arid Environ. 7, 40–47.

Freikman, M., Porat, N., 2017. Rujm el-Hiri: the monument in the landscape. Tel Aviv 44, 14–39.

Fruchter, N., Matmon, A., Avni, Y., Fink, D., 2011. Revealing sediment sources, mixing, and transport during erosional crater evolution in the hyperarid Negev Desert, Israel. Geomorphology 134 (3-4), 363-377.

Galbraith, R.F., Roberts, R.G., 2012. Statistical aspects of equivalent dose and error calculation and display in OSL dating: an overview and some recommendations. Quat. Geochronol. 11, 1–27.

Gliganic, L.H., Cohen, T.J., Meyer, M., Molenaar, A., 2017. Variations in luminescence properties of quartz and feldspar from modern fluvial sediments in three rivers. Quat. Geochronol. 41, 70-82.

Gosse, J.C., Phillips, F.M., 2001. Terrestrial in situ cosmogenic nuclides: theory and application. Quat. Sci. Rev. 20(14), 1475-1560.

Gran, S. E., Matmon, A., Bierman, P.R., Rizzo, D., Enzel, Y., Caffee, M., 2001. Determination of displacement history from a limestone normal fault scarp using cosmogenic ^{36}Cl, northern Israel. J. Geophys. Res. 106 (B3), 4247- 4264.

Gran, K.B., Finnegan, N., Johnson, A.L., Belmont, P., Wittkop, C., Rittenour, T., 2013. Landscape evolution, valley excavation, and terrace development following abrupt postglacial base-level fall. GSA Bulletin 125 (11/12), 1851–1864. doi: 10.1130/B30772.

Granger, D.E., Piccini, L., Kirchner, J.W. Carmignani, L., Fantozzi, P., Meccheri, M., Tavarnelli, E., 1997. Dating exhumation of orogenic belts using cosmogenic isotopes in cave deposits and alluvial terraces. Comitato Glaciologico Italiano Location Italy (ITA) 3, 187-188.

Groos, A.R., Akçar, N., Yesilyurt, S., Miehe, G., Vockenhuber, C., Veit, H., 2021. Nonuniform Late Pleistocene glacier fluctuations in tropical Eastern Africa. Sci. Adv. 7, Issue 11. DOI: 10.1126/sciadv.abb6826.

Grodek, T., 1994. Stair pools -morphology and processes at the upper Meshushim stream, Golan Heights. MSc. Thesis, Department of Physical Geography, Institute of Earth Sciences, Hebrew University of Jerusalem. 90 pp. (In Hebrew).

Guralnik, B., Matmon, A., Avni, Y., Fink, D., 2010. 10Be exposure ages of ancient desert pavements reveal Quaternary evolution of the Dead Sea drainage basin and rift margin tilting. Earth Planet. Sci. Lett. 290 (1-2), 132-141.

Guralnik, B., Matmon, A., Avni, Y., Porat, N., Fink, D., 2011. Constraining the evolution of river terraces with integrated OSL and cosmogenic nuclide data. Quat. Geochronol. 6 (1), 22-32.

Halfon N., Yosef. Y., 2021. Comparison of three standard periods in the amount of rain in Israel, 1931-2020. Report 4000 -The Israeli Meteorological Service 0804-2021-000010. (In Hebrew).

Hancock, G.S., Anderson, R.S., 2002. Numerical modeling of fluvial strath-terrace formation in response to oscillating climate. GSA Bulletin114, (9), 1131-1142.

Hancock, G. S., Anderson, R. S., 2002. Numerical modeling of fluvial strath-terrace formation in response to oscillating climate. GSA Bulletin 114 (9), 1131-1142.

Harbor, J., Warburton, J., 1993. Relative Rates of Glacial and Nonglacial Erosion in Alpine Environments. Arct. Alp. Res. 25(1), 1-7.

Haviv, I., Enzel, Y., Whipple, K.X., Zilberman, E., Stone, J., Matmon, A., Fifield, L.K., 2006. Amplified erosion above waterfalls and oversteepened bedrock reaches. J. Geophys. Res. Earth Surf., 111(F4).

Heimann, A., Steinitz, G., Mor, D., Shaliv, G., 1996. The Cover Basalt Formation, its age and its regional and tectonic setting: implications from K–Ar and 40Ar/39Ar geochronology. Isr. J. Earth Sci. 45, 55–71.

Inbar, M. 1992. Rates of fluvial erosion in basins with a Mediterranean type climate. Catena 19, 393-409.

Inbar, M., 2000. Episodes of flash floods and boulder transport in the Upper Jordan River. The Hydrology-Geomorphology Interface: Rainfall, Floods, Sedimentation, Land-use. Proceedings of the Jerusalem Conference, May 1999. IAHS Publication 261, 185-200.

Inbar, M., 2012. Short-term channel changes after flash floods in the Upper Jordan River, Israel. Horizons in Geography No. 79/80, Themes in Israeli Geography, 26-36.

Inbar, M., Even-Nir, M., 1989. Landslides in the Upper Jordan gorge. Pirineos 134, 23-40.

Inbar, M., Schick, A.P. 1979. Bed-load transport associated with high stream power, Jordan River, Israel. Proc. Nat. Acad. Sci. (PNAS), USA, 76(6), 2515-2717.

Jomelli, V., Lane, T.P., Favier, V., Masson-Delmotte, V., Swingedouw, D., Rinterknecht, V., Schimmelpfennig, I., Schimmelpfennig, D., Verfaillie, D., Adamson, K., Leanni, L., Mokadem, F, ASTER Team, 2016. Paradoxical cold conditions during the medieval climate anomaly in the Western Arctic. Scientific Reports 6, 32984. DOI: 10.1038/srep32984.

Kober, F., Ivy-Ochs, S., Schlunegger, F., Baur, H., Kubik, P.W., Wieler, R., 2007. Denudation rates and a topography-driven rainfall threshold in Northern Chile: multiple cosmogenic nuclide data and sediment yield budgets. Geomorphology 83,97-120. doi:10.1016/j.geomorph.2006.06.029.

Leopold, L.B., Bull W.B., 1979. Base Level, Aggradation, and Grade. Proc. Am. Philos. Soc. (123), 168-202.

Licciardi, J.M., Denoncourt,C.L., Finkel, R.C., 2008. Cosmogenic 36Cl production rates from Ca spallation in Iceland. Earth. Planet. Sci. Lett. 267 (1-2), 365-377.

Madsen A.T., Murray, A.S., 2009. Optically stimulated luminescence dating of young sediments: A review. Geomorphology 109 (1-2), 3-16.

Marrero, S.M., Phillips, F.M., Caffee, M.W., Gosse, J.C., 2016. CRONUS-Earth cosmogenic 36Cl calibration. Quat. Geochronol. 31, 199-219. ISSN 1871-1014, https://doi.org/10.1016/j.quageo.2015.10.002.

Matmon, A., Bierman, P.R., Larsen, J., Southworth, S., 2003. Temporally and spatially uniform rates of erosion in the southern Appalachian Great Smoky Mountains. Geology 31 (2), 155-158.

Matmon, A., Simhai, O., Amit, R., Haviv, I., Porat, N., 2009. Desert pavement–coated surfaces in extreme deserts present the longest-lived landforms on Earth. Geol. Soc. Am. Bull. 121 (5-6), 688-697.

Matmon, A., Elfassi, S., Hidy, A., Geller, Y., Porat, N., 2016. Controls on aggradation and incision in the NE Negev, Israel, since the middle Pleistocene. Geomorphology 261, 132-146.

Matmon, A., 2017. Cosmogenic isotope-based erosion rates along the western margin of the Dead Sea fault. Invited review paper, in: eds.: Enzel, Y., and Bar Yosef, O. The Quaternary of the Levant, Cambridge University Press.

Molnar, P., England, P., 1990. Late Cenozoic uplift of mountain ranges and global climate change: chicken or egg?. Nature 346, 29–34. https://doi.org/10.1038/346029a0.

Meiler, M., Reshef, M., Shulman, H., 2011. Seismic depth-domain stratigraphic classification of the Golan Heights, central Dead Sea Fault. Tectonophysics 510, 354–369.

Merchel, S., Bremser, W., Alfimov, V., Arnold, M., Aumaître, G., Benedetti, L., Bourlès, D.L., Caffee, M., Fifield, L.K., Finkel, R.C., Freeman, S.P.H.T., Martschini, M., Matsushi, Y., Rood, D.H., Sasa, K., Steier, P., Takahashi, T., Tamari, M., Tims, S.G., Tosaki, Y., Wilcken, K.M., Xu, S., 2011. Ultra-trace analysis of ^{36}Cl by accelerator mass spectrometry: an interlaboratory study. Anal. Bioanal. Chem. 400, 3125–3132. https://doi.org/10.1007/s00216-011-4979-2

Mozafari, N., Sümer, Ö., Tikhomirov, D., Ivy-Ochs, S., Alfimov, V., Vockenhuber, C., Inci U., Sözbilir, U., Akcar, N., 2019. Holocene seismic activity of the Priene-Sazlı Fault revealed by cosmogenic ^{36}Cl, western Anatolia, Turkey. Turk. J. Earth Sci. 28, 410-437.

Mor, D., 1993. A time-table for the Levant Volcanic Province, according to K–Ar dating in the Golan Heights. Isr. J. Afr. Earth Sci. 16, 223–234.

Neagu, N., Matmon, A., Enzel, Y, Porat, N., 2020. Quaternary evolution of a hyperarid drainage under climatic fluctuations and rift-margin base-level fall, NE Negev, Israel. Geomorphology 354 (6), 107042. DOI:10.1016/j.geomorph.2020.107042.

Nishiizumi, K., Caffee, M.W., Finkel, R.C., Brimhall, G., Mote, T.,2005. Remnants of a fossil alluvial fan landscape of Miocene age in the Atacama Desert of Northern Chile using cosmogenic nuclide exposure age dating. Earth Planet. Sci. Lett. 237, 499–507. doi:10.1016/j.epsl.2005.05.032

Palumbo, L., Benedetti, L., Bourles, D., Cinque, A., Finkel, R., 2004. Slip history of the Magnola fault (Apennines, Central Italy) from ^{36}Cl surface exposure dating: evidence for strong earthquakes over the Holocene. Earth Planet. Sci. Lett. 225(1-2), 163-176.

Pazzaglia, F.J., 2013. Fluvial Terraces, in: Treatise on Geomorphology 9, 379–412, https://doi.org/10.1016/B978-0-12-374739-6.00248-7.

Perron, J.T., 2017. Climate and the Pace of Erosional Landscape Evolution: Ann. Rev. Earth Planet. Sci. 45, 561–591. doi.org/10.1146/annurev-earth-060614-105405.

Phillips, F.M., Zreda, M.G., Smith, S.S., Elmore, D., Kubik, P.W., Sharma, P., 1990. Cosmogenic Chlorine-36 Chronology for Glacial Deposits at Bloody Canyon, Eastern Sierra Nevada. Science, New Series 248 (4962), 1529-1532.

Porat, N., Duller, G.A.T., Roberts, H.M., Piasetzky, E., Finkelstein, I., 2012. OSL dating in multi-strata Tel: Megiddo (Israel) as a case study. Quat. Geochronol. 10, 359–366.

Portenga, E.W., Bierman, P.R., 2011. Understanding Earth's eroding surface with ^{10}Be. GSA Today 21(8):4-10. DOI: 10.1130/G111A.1

Riebe, C.S., Kirchner, J.W., Granger, D.E., and Finkel, R.C., 2001. Strong tectonic and weak climatic control of long-term chemical weathering rates. Geology 29, 511–514.

Rinat, Y., Matmon, A., Arnold, M., Aumaître, G., Bourlès, D., Ked-dadouche, K., Porat, N., Morin, E., Finkel, R.C., 2014. Holocenerockfalls in the southern Negev Desert, Israel and their relationto Dead Sea fault earthquakes. Quat. Res. 81, 260–273. doi:10.1016/j.yqres.2013.12.008.

Ryb, U., Matmon, A., Erel, Y., Haviv, I., Katz, A., Starinsky, A., Angert, A., ASTER Team, 2014a. Controls on denudation rates in tectonically stable Mediterranean carbonate terrain. Geol. Soc. Am. Bull. 126(3-4), 553-568.

Ryb, U., Matmon, A., Erel, Y., Haviv, I., Benedetti, L., Hidy, A.J., 2014b. Styles and rates of long-term denudation in carbonate terrains under a Mediterranean to hyper-arid climatic gradient. Earth Planet. Sci. Lett. 406, 142-152.

Schimmelpfennig, I., 2009. Cosmogenic Cl-36 in Ca and K rich minerals: analytical developments, production rate calibrations and cross calibration with He-3 and Ne-21. Applied geology. Université Paul Cézanne - Aix-Marseille III, 2009. English.

Schimmelpfennig, I., Benedetti, L., Finkel, R., Pik, R., Blard, P. H., Bourles, D., Burnard P., Williams, A., 2009. Sources of in-situ ^{36}Cl in basaltic rocks. Implications for calibration of production rates. Quat. Geochronol. 4(6), 441-461.

Schimmelpfennig, I., Benedetti, L., Garreta, V., Pik, R., Blard, P. H., Burnard, P., Bourle`s, D., Finnkel, R., Ammon, K., Dunai, T., 2011. Calibration of cosmogenic ^{36}Cl production rates from Ca and K spallation in lava flows from Mt. Etna (38° N, Italy) and Payun Matru (36° S, Argentina). Geochim. Cosmochim. Acta. 75(10), 2611-2632.

Schimmelpfennig, I., Schaefer, J.M., Putnam, A.E., Koffman, T., Benedetti, L., Ivy-Ochs, S., ASTER TEAM, Schluchter, C., 2014. ^{36}Cl production rate from K-spallation in the EuropeanAlps (Chironico landslide, Switzerland). J. Quaternary Sci. 29, 407-413.

Schlagenhauf, A., Gaudemer, Y., Benedetti, L., Manighetti, I., Palumbo, L., Schimmelpfennig, I., Finkel, R., Pou, K., 2010. Using in situ Chlorine-36 cosmonuclide to recover past earthquake histories on limestone normal fault scarps: a reappraisal of methodology and interpretations. Geophys. J. Int. 182 (1), 36–72.

Schumm, S.A., 1973. Geomorphic Thresholds and Complex Response of Drainage Systems. In: Morisawa, M., Ed., Fluvial Geomorphology, Publications of Geomorphology, State University of New York, Binghamton, 299-310.

Schumm S.A., 1981. Evolution and response of the fluvial system, Sedimentologic implications. Soc. Economic Paleontologists and Mineralogists Spec. Pub. 31, pp. 19–29.

Schumm, S.A., Lichty, R.W., 1965. Time, space and causality in geomorphology. Am. J. Sci. 263, 110-19.

Sklar, L.S., Dietrich, W.E., 2001. Sediment and rock strength controls on river incision into bedrock. Geology, 29 (12), 1087. doi:10.1130/0091-7613(2001)029<1087:sarsco>2.0.co;2

Stone, J.O., 2000. Air pressure and cosmogenic isotope production. J. Geophys. Res. 105, 23,753–759.

Stone, J.O., Fifield, K., Vasconcelos, P., (2005). Terrestrial chlorine-36 production from spallation of iron. In: Abstract of 10th International Conference on Accelerator Mass Spectrometry.

Thomas, F., Godard, V., Bellier, O., Shabanian, E., Ollivier, V., Benedetti, L., Rizza, M., Espurt N., Hollender, F., Guillou, V., Molliex, S., ASTER Team (2017). Morphological controls on the dynamics of carbonate landscapes under a Mediterranean climate. Terra Nova, 29(3), 173-182.

Weinstein, Y., Navon, O., Altherr, R., Stein, M., 2006. The role of lithospheric mantle heterogeneity in the generation of Plio-Pleistocene alkali basaltic suites from NW Harrat Ash Shaam (Israel). J. Petrol. 47 (5), 1017–1050.

Weinstein, Y., Nuriel, P., Inbar, M., Jicha, B.R., Weinberger, R. (2020). Impact of the dead sea transform kinematics on adjacent volcanic activity. Tectonics 39 (1), e2019TC005645.

Zilberman, E., Amit, R., Heimann, A., Porat, N. (2000). Changes in Holocene Paleoseismic activity in the Hula pullapart basin, Dead Sea Rift, northern Israel. Tectonophysics 321, 237–252.

Zreda M. G., Phillips F. M., Elmore D., Kubik P. W., Sharma P. and Dorn R. I. (1991) Cosmogenic chlorine-36 production rates in terrestrial rocks. Earth Planet. Sci. Lett. 105, 94–109.

Declaration of interests

☒ The authors declare that they have no known competing financial interests or personal relationships that could have appeared to influence the work reported in this paper.

☐ The authors declare the following financial interests/personal relationships which may be considered as potential competing interests:

Highlights

- Cosmogenic ^{36}Cl in bedrock and sediments of basaltic terrain, N Dead Sea Rift (DSR)
- ^{36}Cl -based calculated denudation ages compatible with range of other DSR studies
- Chemical weathering at bedrock-soil interface controls most of erosion
- Soil cover residence time up to several thousands of years consistent with OSL ages
- Present denudation and sediment yield lower than during most of the Holocene

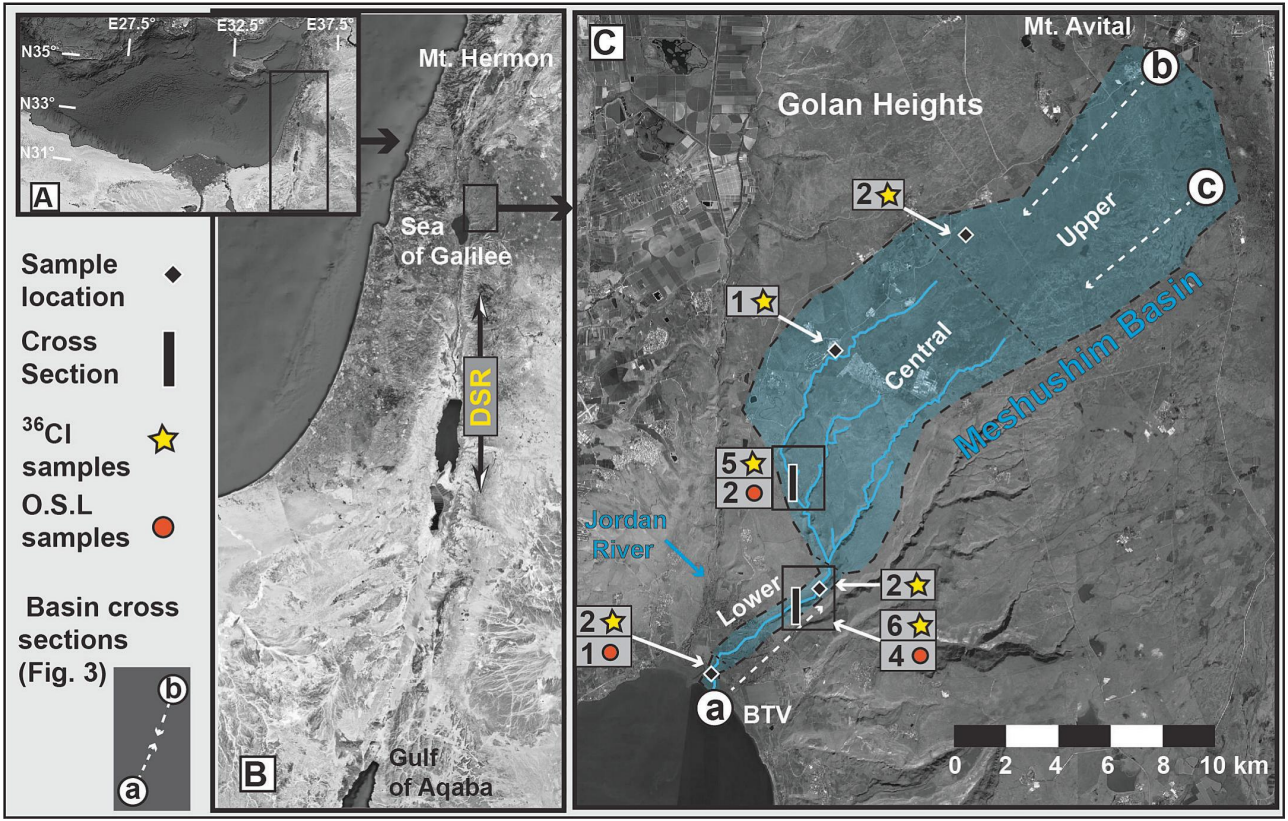
E27.5°
E32.5°
E37.5°
N35°
N33°
N31°
A
Mt. Hermon
Sea of Galilee
DSR
B
Gulf of Aqaba
Sample location
Cross Section
36Cl samples
O.S.L samples
Basin cross sections (Fig. 3)
b
a
C
Mt. Avital
Golan Heights
b
c
2
Upper
1
Central
Meshushim Basin
5
2
Jordan River
Lower
2
6
4
2
1
a
BTV
0 2 4 6 8 10 km

Figure 1

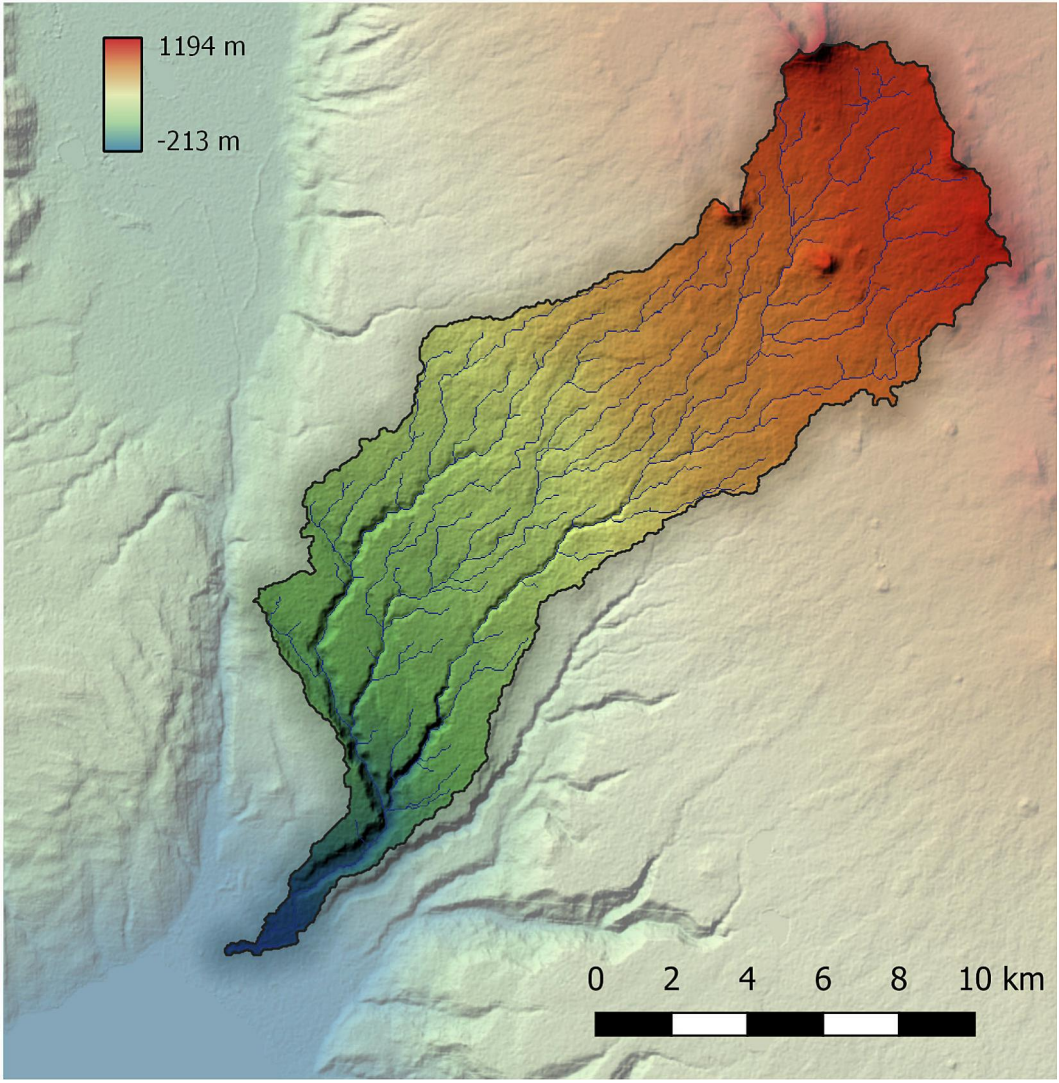

Figure 2

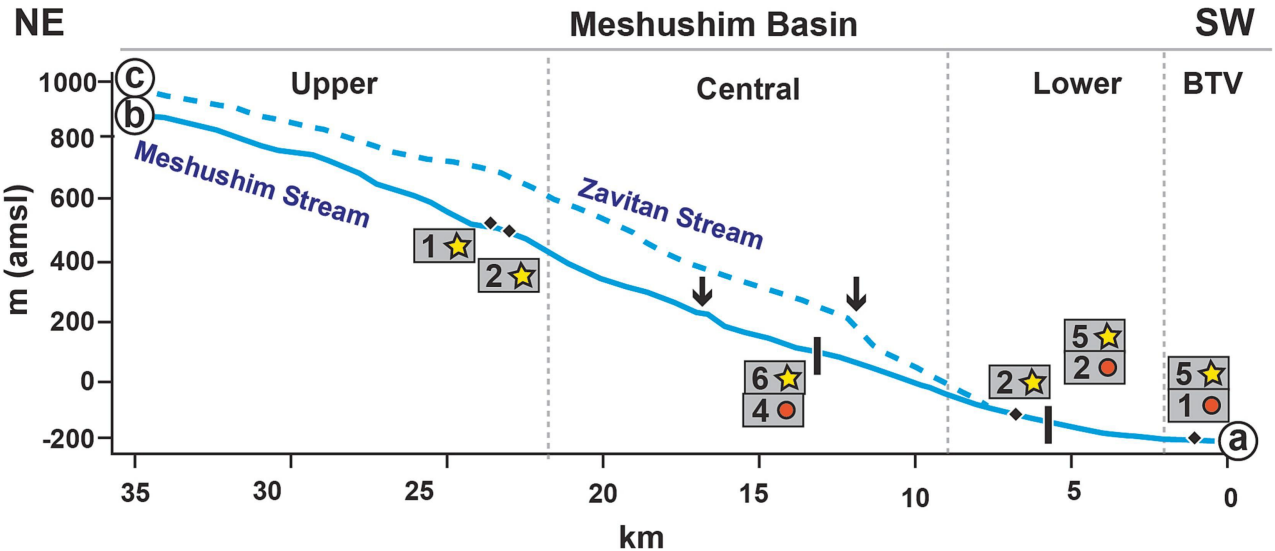
NE
Meshushim Basin
SW
Upper
Central
Lower
BTV
c
b
a
Meshushim Stream
Zavitan Stream
1
2
6
4
2
5
2
5
1
1000
800
600
400
200
0
-200
m (amsl)
35
30
25
20
15
10
5
0
km

Figure 3

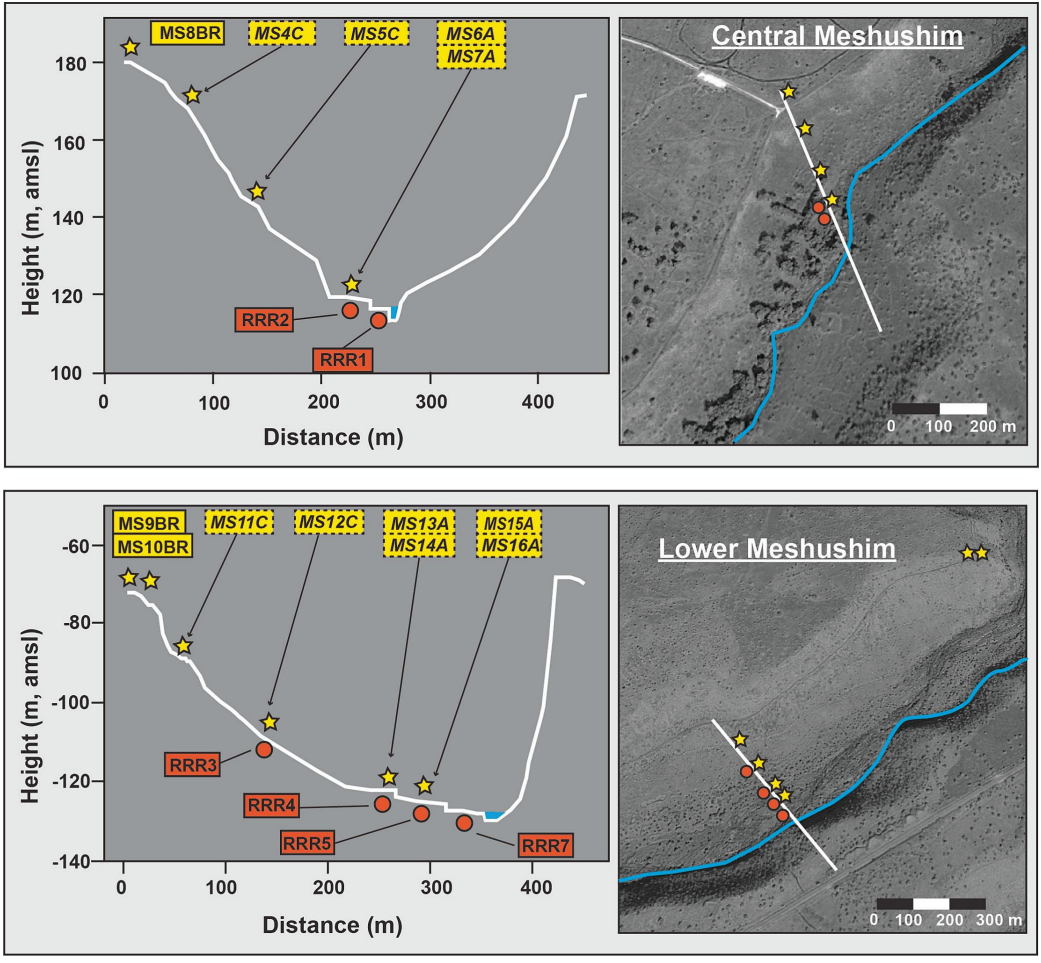
MS8BR
MS4C
MS5C
MS6A
MS7A
RRR2
RRR1
Height (m, amsl)
Distance (m)
Central Meshushim
0 100 200 m
MS9BR
MS10BR
MS11C
MS12C
MS13A
MS14A
MS15A
MS16A
RRR3
RRR4
RRR5
RRR7
Lower Meshushim
0 100 200 300 m

Figure 4

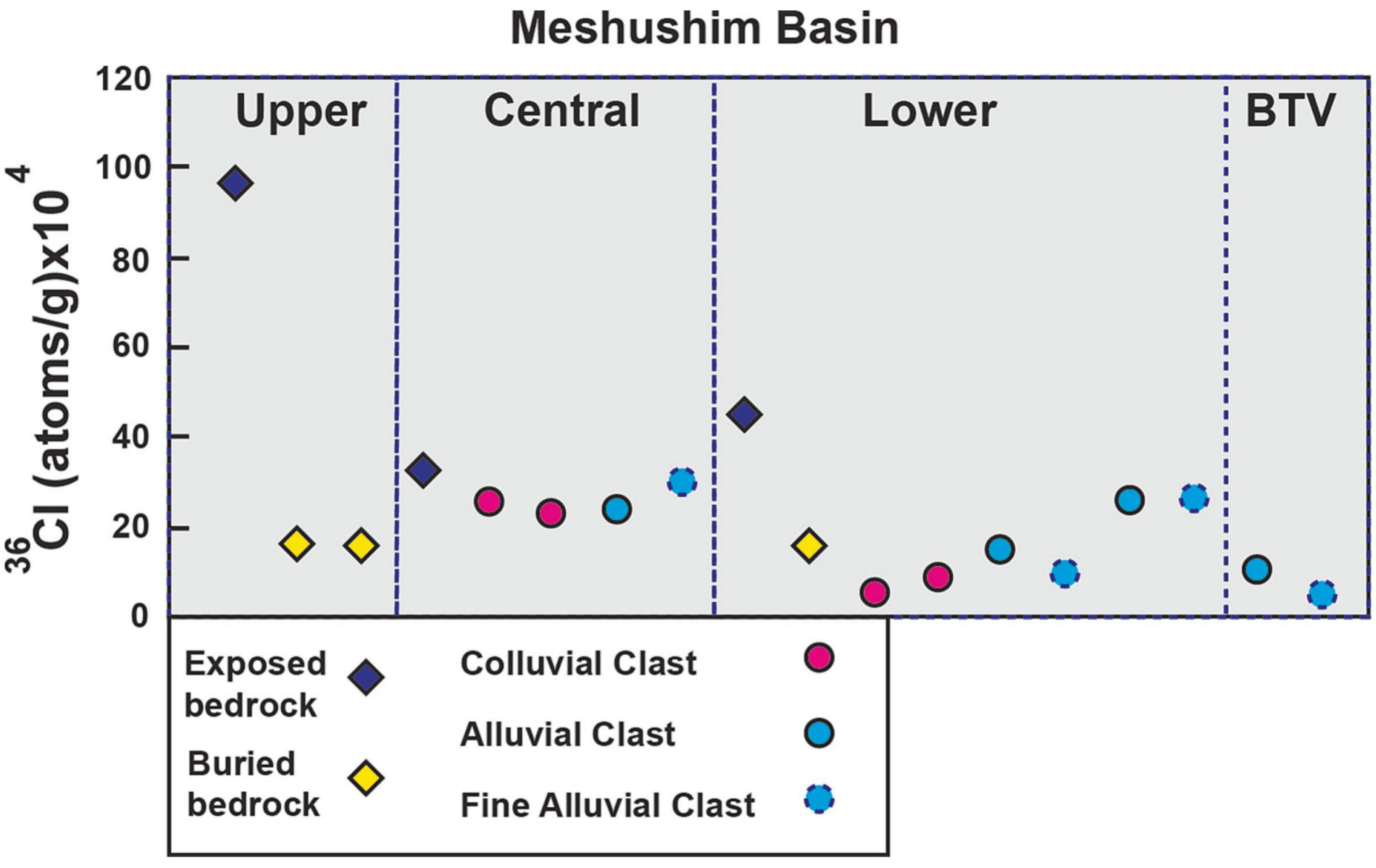
Meshushim Basin
Upper
Central
Lower
BTV
120
100
80
60
40
20
0
^{36}Cl (atoms/g)x10^{4}
Exposed bedrock
Buried bedrock
Colluvial Clast
Alluvial Clast
Fine Alluvial Clast

Figure 5

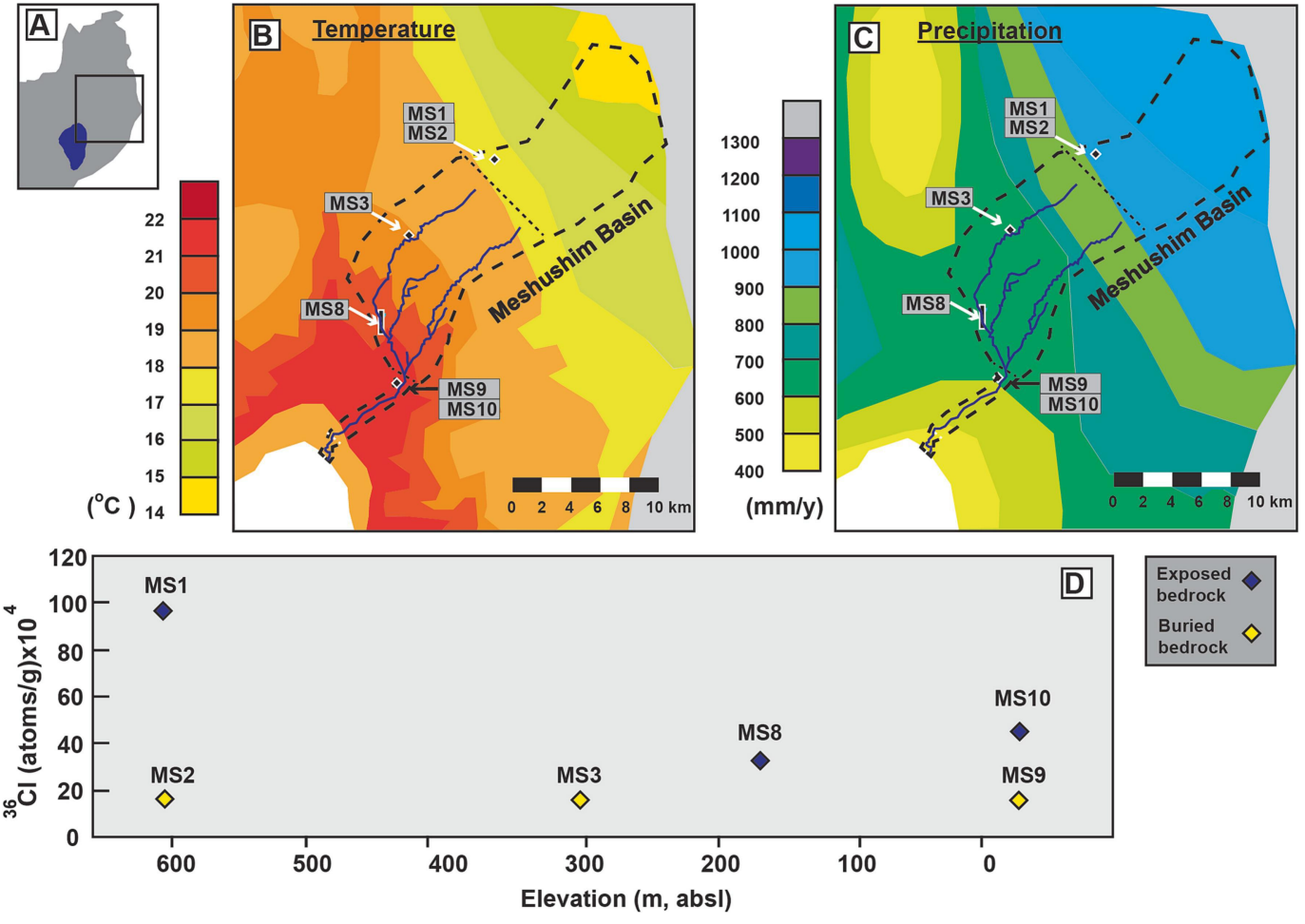
A
B
Temperature
MS1
MS2
MS3
MS8
MS9
MS10
Meshushim Basin
22
21
20
19
18
17
16
15
14
(°C)
0 2 4 6 8 10 km
C
Precipitation
1300
1200
1100
1000
900
800
700
600
500
400
(mm/y)
D
Exposed bedrock
Buried bedrock
^{36}Cl (atoms/g)x10^{4}
120
100
80
60
40
20
0
600
500
400
300
200
100
0
Elevation (m, absl)

Figure 6

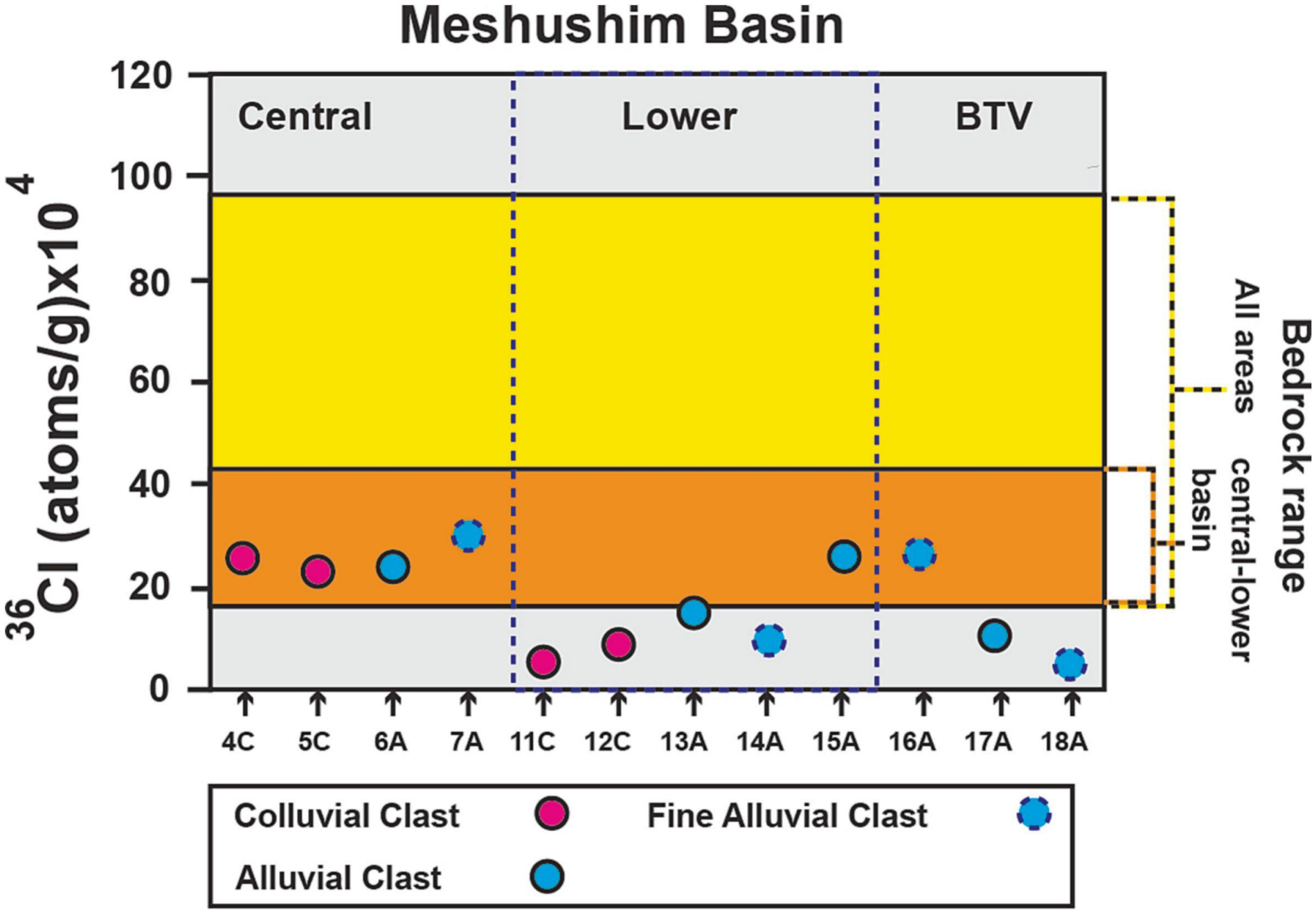
Meshushim Basin
120
100
80
60
40
20
0
^{36}Cl (atoms/g)x10^{4}
Central
Lower
BTV
All areas
central-lower basin
Bedrock range
4C
5C
6A
7A
11C
12C
13A
14A
15A
16A
17A
18A
Colluvial Clast
Fine Alluvial Clast
Alluvial Clast

Figure 7

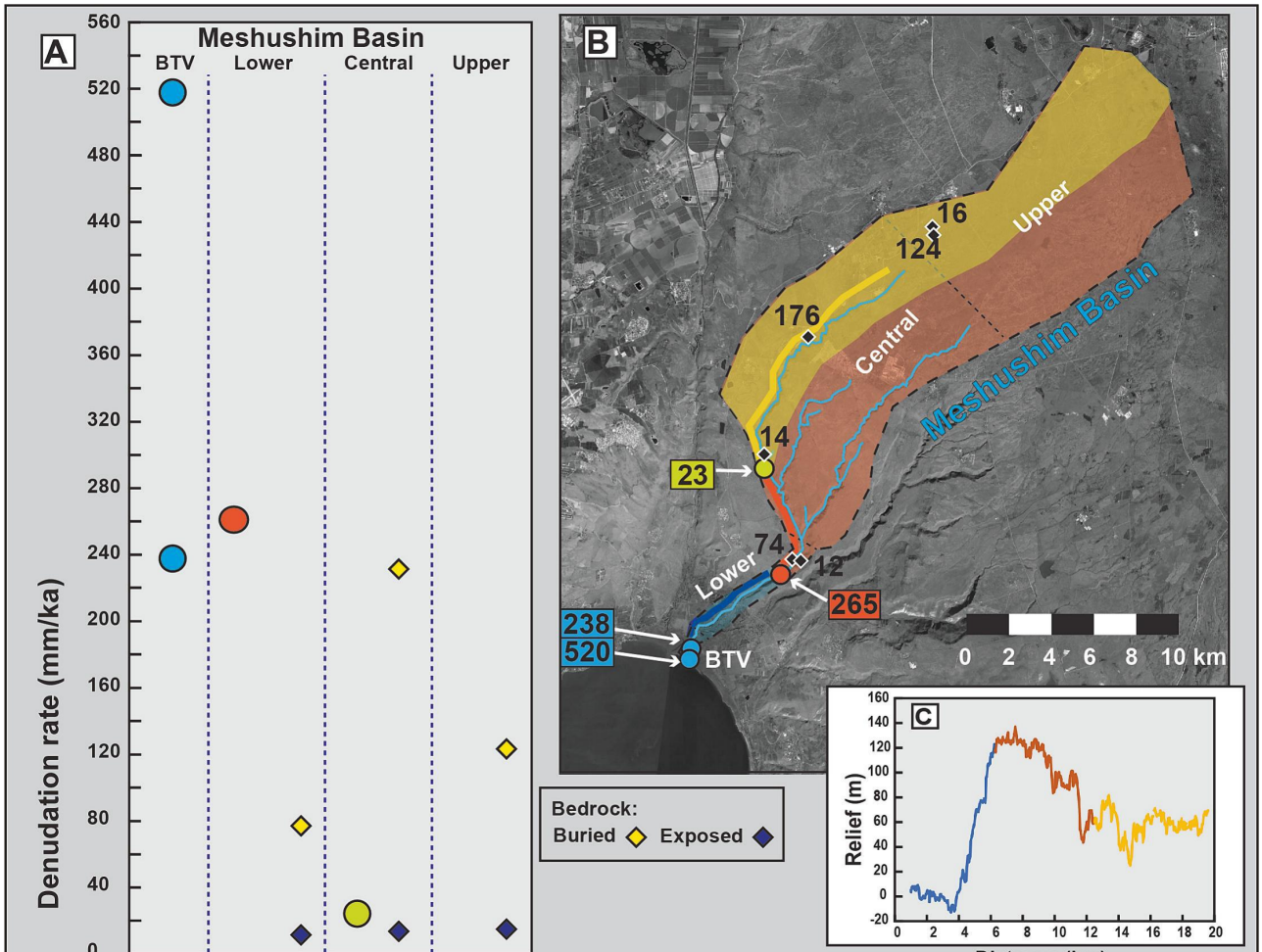
A
Meshushim Basin
BTV
Lower
Central
Upper
Denudation rate (mm/ka)
560
520
480
440
400
360
320
280
240
200
160
120
80
40
0
B
16
124
Upper
176
Central
Meshushim Basin
14
23
74
12
Lower
265
238
520
BTV
0 2 4 6 8 10 km
Bedrock:
Buried
Exposed
C
Relief (m)
160
140
120
100
80
60
40
20
0
-20
0 2 4 6 8 10 12 14 16 18 20
Distance (km)

Figure 8

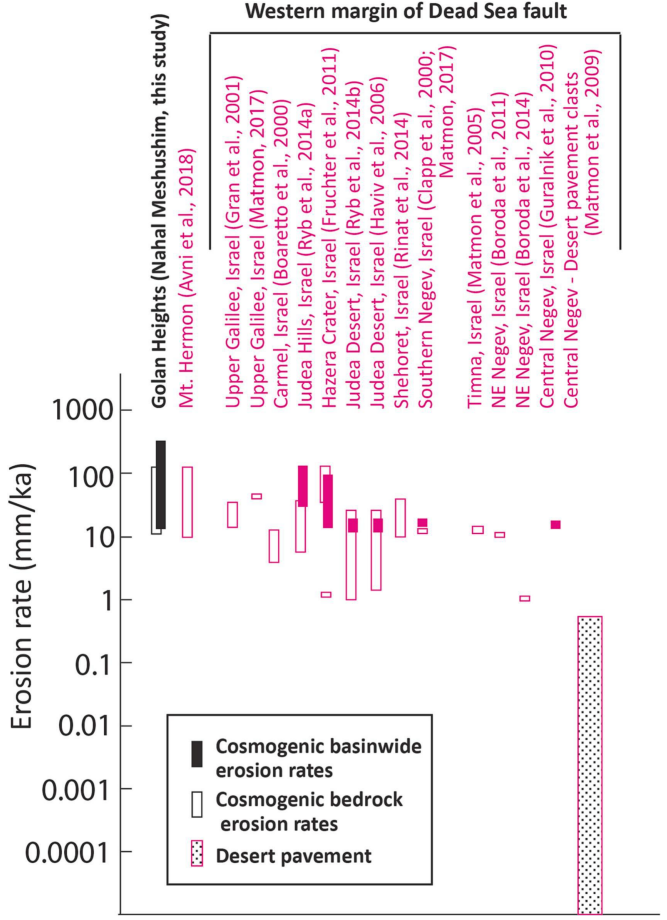
Western margin of Dead Sea fault
Golan Heights (Nahal Meshushim, this study)
Mt. Hermon (Avni et al., 2018)
Upper Galilee, Israel (Gran et al., 2001)
Upper Galilee, Israel (Matmon, 2017)
Carmel, Israel (Boaretto et al., 2000)
Judea Hills, Israel (Ryb et al., 2014a)
Hazera Crater, Israel (Fruchter et al., 2011)
Judea Desert, Israel (Ryb et al., 2014b)
Judea Desert, Israel (Haviv et al., 2006)
Shehoret, Israel (Rinat et al., 2014)
Southern Negev, Israel (Clapp et al., 2000; Matmon, 2017)
Timna, Israel (Matmon et al., 2005)
NE Negev, Israel (Boroda et al., 2011)
NE Negev, Israel (Boroda et al., 2014)
Central Negev, Israel (Guralnik et al., 2010)
Central Negev - Desert pavement clasts (Matmon et al., 2009)
Erosion rate (mm/ka)
1000
100
10
1
0.1
0.01
0.001
0.0001
Cosmogenic basinwide erosion rates
Cosmogenic bedrock erosion rates
Desert pavement

Figure 9